

Section 1

**Atmospheric data assimilation schemes, analysis
and initialization, data impact studies,
observing system experiments**

A study of the flow-dependence of background error covariances based on the NMC method

Harald Anlauf¹, Werner Wergen and Gerhard Paul

Deutscher Wetterdienst, Offenbach, Germany

Modern data assimilation systems such as the 4D-Var and the Ensemble Kalman Filter (EnKF) use the dynamics of the forecast model to evolve the covariance matrix of background error \mathbf{B} in time either implicitly (4D-Var) or explicitly (EnKF). As a consequence, these schemes effectively use flow-dependent structure functions [1], although at correspondingly high computational costs. Nevertheless, the initial \mathbf{B} -matrix still has to be specified, like for any simpler assimilation system (e.g., OI, 3D-Var). The 4D-Var also does not transfer the dynamical background covariances to subsequent assimilations.

In order to explore the variability of the \mathbf{B} -matrix with respect to flow pattern explicitly, we applied the NMC method at DWD to the global model GME. The NMC method uses differences of short-range forecasts verifying at the same time but with different starting dates as proxies for background error. The method assumes that the spatial structure of background error does not strongly vary with forecast time, so that the correlations obtained from forecast differences are reasonable approximations to the true background error correlations, at least for the mid-latitudes.

For the present study we used the differences of 48h and 24h forecasts of geopotential height verifying at 00Z during the winter period from Dec. 1, 2003, until Feb. 29, 2004. The forecast fields were taken from the archived main runs of the operational GME model. The evaluation of covariances shown here was performed on a regular grid at fixed reference latitude and with zonal averaging. The isotropic part of the empirical correlation of geopotential height of the 500 hPa surface at 45°N is shown as the blue curve in fig. 1.

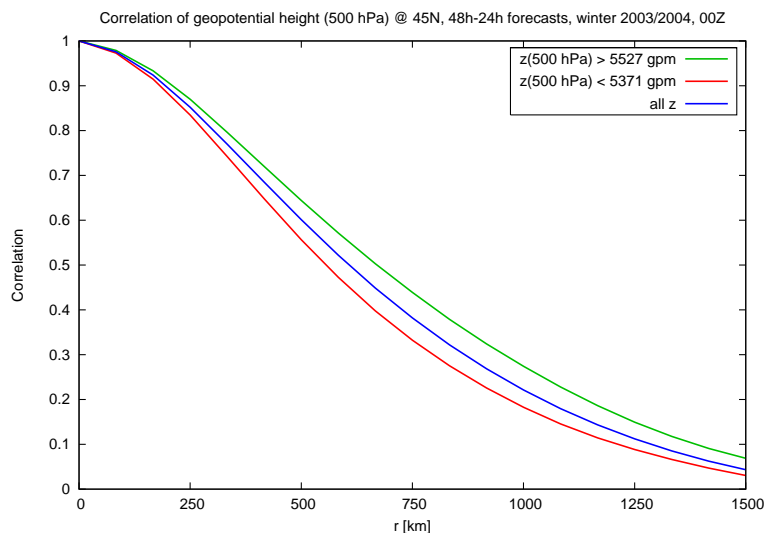


Figure 1: Correlation of the 500 hPa height from 48h–24h forecast differences

¹harald.anlauf@dwd.de

For the exploration of the flow-dependence, we took the 24h forecast of the 500 hPa height as an indicator for the meteorological situation. Based on the statistics of the geopotential height at fixed latitude over the whole period, we distributed the contributions into three classes of approximately equal sample sizes. For our forecast sample and at 45°N, a data point was associated with a region of “high” and “low” pressure if $z(500 \text{ hPa}) > 5527 \text{ gpm}$ and $z(500 \text{ hPa}) < 5371 \text{ gpm}$, resp., otherwise it was assigned to the “neutral” class. The resulting horizontal correlation functions obtained from contributions in the classes “high” and “low” are shown in fig. 1 as green and red curves. Clearly the correlations for “high” are significantly broader than for “lows”.

We extended the above analysis also to other pressure levels. In order to keep a uniform criterion for the selection of meteorological situations, we chose the geopotential height of the co-located 500 hPa surface. The corresponding dependence of the horizontal correlation scale on vertical level is shown in fig. 2. The data demonstrate that there clearly is a considerable variation of correlation scale with flow pattern.

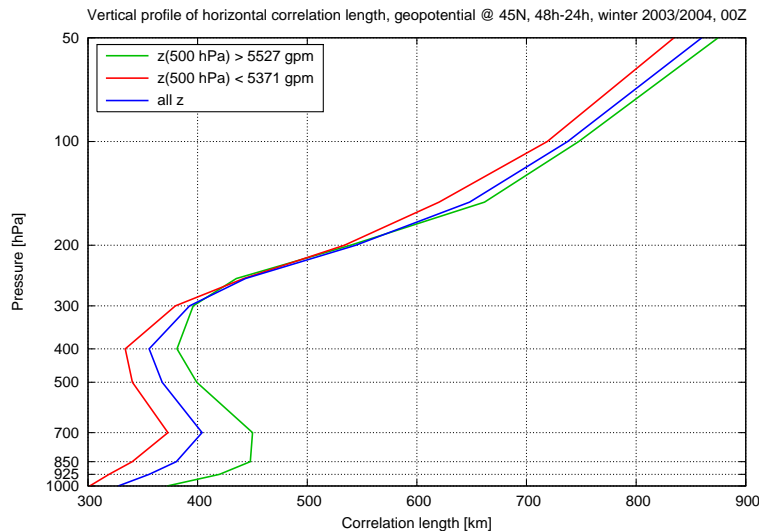


Figure 2: Vertical profile of the horizontal correlation scale of geopotential

We have also analyzed the flow-dependence of cross-correlations with other forecast fields and vertical correlations, as well as the variation with location and season. The corresponding results will be presented elsewhere.

References

- [1] J.-N. Thépaut, P. Courtier, G. Belaud and G. Lemaître, *Dynamical structure functions in a four-dimensional variational assimilation: A case study*, Q. J. R. Meteorol. Soc. **122** (1996) 535-561.

A prototype of the Canadian Land Data Assimilation System and its application to soil moisture analysis.

G. Balsamo, J.-F. Mahfouf, S. Bélair and G. Deblonde

Meteorological Service of Canada, Meteorological Research Branch

Abstract

The Canadian Land Data Assimilation System (CaLDAS) combines land surface modelling capabilities with optimal estimation data assimilation techniques to provide a reliable land surface analysis as initial condition in weather and climate prediction at the Meteorological Service of Canada (MSC). A first application of CaLDAS focused on soil moisture since it can strongly affect atmospheric low level temperature and humidity via the partitioning of latent and sensible heat fluxes at the surface. The assimilation of different sources of data is investigated for the production of a daily soil moisture analysis, with the aid of Observing System Simulated Experiments (OSSEs). In the CaLDAS OSSEs we consider the assimilation of ground-based observations (SYNOP temperature and humidity), current available satellite observations (AQUA and GOES satellites), and observations provided in the future (by SMOS and Hydros satellites). A prototype of CaLDAS is described and perspectives of implementation at MSC are briefly discussed.

The land surface modelling

The parameterization schemes in CaLDAS can be separated into three main components: (1) the land surface scheme (ISBA, Noilhan and Planton, 1989, Noilhan and Mahfouf, 1996) which simulates the evolution of the land surface state, (2) the atmospheric driver which provides the necessary forcing at the surface (i.e. precipitation, radiation, etc.), and (3) the observation operator (i.e. a radiative transfer model) which simulates a given observable (i.e. a brightness temperature) informative on the variable to be initialized (i.e. soil moisture). The first two components of the system are part of the operational code at MSC, while the observation operator has been implemented for both infrared and microwave frequencies. A microwave radiative transfer model (LSMEM, Drusch et al. 2001) is used to simulate land microwave emission, while for infra-red a uniform emissivity approximation is used to calculate a surface skin temperature in clear-sky conditions. In the so-called "off-line" implementation of CaLDAS, the atmospheric forcing is provided to the MEC model, a simplified version of GEM (Côté et al., 1998) where only the land surface and the atmospheric surface boundary layer (Delage, 1997) parameterizations are activated. In the "atmospheric coupled" mode the GEM model itself is used to provide the sensitivities to soil moisture, and it accounts for the components (1) and (2) previously listed.

The data assimilation scheme

The data assimilation scheme for the land surface follows the formulation of Mahfouf (1991) generalized to different observations in Balsamo et al. (2004). A daily soil moisture analysis is performed using a simplified variational scheme where the observation operator is estimated from finite differences. The assimilation system considers a set of indirect observations which are informative on soil moisture and available in a 24-hour time-window. A linear estimate of the observation operator is calculated as sensitivity of the generic observable Y to the initial perturbation of soil moisture ($\Delta Y(t = t_i) / \Delta W_p(t = t_0)$), according to the perturbation method described in Balsamo et al. (2004,b) for the following observations: the microwave brightness temperatures at L-band (1.4 GHz), $T_{b,H}(L)$ and $T_{b,V}(L)$ (horizontal and vertical polarizations) and C-band (6.9 GHz), $T_{b,H}(C)$ and $T_{b,V}(C)$, the clear-sky infra-red skin temperature $T_s(IR)$, and the screen-level temperature T_{2m} and humidity Q_{2m} . A simulation of satellites overpasses according to the specified orbital parameters allows to account for a realistic temporal and spatial availability of the observations.

Results over North America

A set of Observing System Simulated Experiments is performed over North America in order to assess the impact of the different observations types. The two implementations of CaLDAS (MEC "off-line" and

GEM "atmospheric coupled") are applied over a case study selected for the 5th July 2004. A complete set of simulated observations are assimilated to correct a prescribed initial soil moisture error. In Figure 1 is shown the gain matrix element used to assimilate microwave L-band observations (at 12 UTC) as observed in the future by Hydros satellite (Entekhabi et al., 2004). The main structures of the gain

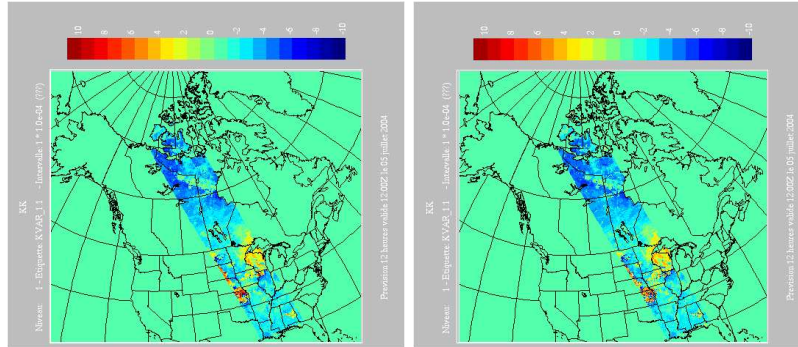


Figure 1: Gain matrix element ($\Delta T_b^H(L)/\Delta W_p [K \cdot m^3 m^{-3}]$) for Hydros L-band simulated observation on the 5th July 2004 at 12 UTC: Off-line (*left*) vs. atmospheric coupled (*right*) estimates.

matrix element for assimilating the L-band brightness temperature are preserved and comparable in both implementations. An objective validation of this equivalence for each observation source considered is obtained applying the information content diagnostics (Cardinali et al., 2004), which confirms a similar observation "weight" given by the analysis as shown in Figure 2.

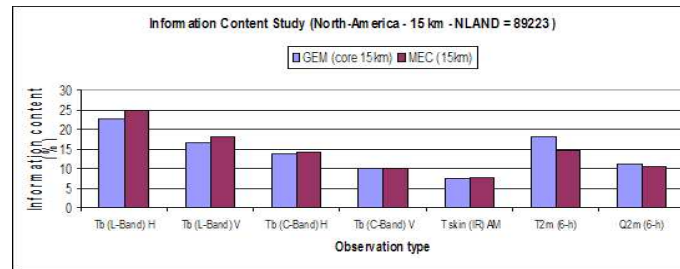


Figure 2: Information content study over CaLDAS North American domain: GEM (*left*) vs. MEC (*right*).

Conclusions and Perspectives

A first prototype of the CaLDAS system is being tested for the analysis of soil moisture via the simplified variational assimilation of different observations types. The equivalence of "off-line" and "atmospheric coupled" approaches introduces the possibility to use a separate land surface modelling system, while preserving the consistency with the operational land surface state. The off-line setup of CaLDAS has a considerable advantage of a drastically reduced computational cost, allowing for the investigation of a more complex data assimilation scheme (i.e. Ensemble Kalman Filter), land surface scheme (i.e. multi-layer/multi-budget schemes) and the extension of the analysis to other relevant land surface variables (i.e. snow and vegetation). A first implementation of the system will consider, in the near future, the available screen-level observations both at synoptic and asynoptic hours.

References

Balsamo G., Bouyssel F., Noilhan J., Mahfouf J.-F., Bélair S., Deblonde G. (2004) A simplified variational analysis scheme for soil moisture: Developments at Meteo-France and MSC. *Proc. ECMWF/ELDAS workshop on land surface assimilation. Reading, 8-11 November 2004.*

Missing ref. at www.ecmwf.int/publications/library/ecpublications/_pdf/workshop/2004/ws-ELDAS-balsamo.pdf

Assimilation of infrared limb radiances from MIPAS in the ECMWF system

Niels Bormann¹, Sean B. Healy, and Marco Matricardi
European Centre for Medium-range Weather Forecasts
Shinfield Park, Reading, RG2 9AX, UK

ECMWF is developing the capability to directly assimilate radiances from limb sounders in a global data assimilation system. It is the first time that direct assimilation of limb radiances has been attempted. The prototype developments are being carried out for the Michelson Interferometer for Passive Atmospheric Sounding (MIPAS), onboard the Envisat satellite (e.g., European Space Agency, ESA, 2000). MIPAS is a very high spectral resolution interferometer (0.025 cm⁻¹, unapodised), measuring infrared limb radiances in 5 spectral bands between 685 and 2410 cm⁻¹, providing a total of 59,605 spectral points (i.e., channels). In normal scanning mode, MIPAS provides observations at 17 tangent heights in the range of 6-68 km, with a field of view of 3 km in the vertical at the tangent point.

As a first step for the assimilation, a new fast radiative transfer model to compute MIPAS radiances has been developed and validated (Bormann et al. 2004). The model, referred to as RTMIPAS, uses the regression-based methodology of RTTOV (e.g., Saunders et al. 1999), commonly used for nadir radiance assimilation at NWP centres. RTMIPAS can simulate the effect of variable water vapour and ozone; for other gases included in the model a fixed climatological profile is assumed. Tangent linear and adjoint versions of the model have also been developed.

RTMIPAS can reproduce radiances calculated with a line-by-line (LBL) model to an accuracy that is below the noise-level of the instrument for most spectral points and tangent heights (Figure 1), while offering significantly more rapid radiance calculations compared to currently available radiative transfer models. The comparison of RTMIPAS transmittances with LBL equivalents indicates that the accuracy of the RTMIPAS transmittance model is comparable to that of similar regression-based radiative transfer models for the Earth-looking geometry. First comparisons of real MIPAS observations with RTMIPAS-simulated radiances from ECMWF short-term forecasts show differences in line with expected values given the error characteristics of the observations, RTMIPAS, and the forecast data.

A set of MIPAS channels/tangent heights has been selected for assimilation studies and the information content of the selected data relative to the NWP background has been characterised. This shows that assimilation of MIPAS radiances has the potential to significantly reduce the expected analysis error of temperature in the stratosphere and lower mesosphere above about 30 km. For water vapour and ozone, MIPAS can add significant information to the background fields throughout the stratosphere and lower mesosphere. Offline evaluation of MIPAS observations with a 1-dimensional variational (1DVAR) assimilation scheme show encouraging results with impact of MIPAS radiances in regions as expected from the information content studies.

RTMIPAS has been implemented as a new observation operator in the ECMWF system, and assimilation trials will commence shortly. The first implementation assumes local horizontal homogeneity for the limb radiance calculations, but work is also in progress to use a 2-dimensional version of RTMIPAS, allowing a more accurate representation of the limb viewing plane. Simulation studies have shown that a 2-dimensional operator is expected to result in lower errors for the

¹ Email: n.bormann@ecmwf.int

observation operator for more strongly absorbing MIPAS channels and views with lower tangent heights. Also, a 2-dimensional operator may lead to an altered and more adequate horizontal structure of the analysis increments from MIPAS radiances.

Bormann, N., M. Matricardi, and S.B. Healy, 2004: RTMIPAS: A fast radiative transfer model for the assimilation of infrared limb radiances from MIPAS. ECMWF Technical Memorandum No 436, ECMWF, Reading, UK., 49 pp [to appear in *Quart.J.Roy.Meteor.Soc.*].

Saunders, R., M. Matricardi, and P. Brunel, 1999: An improved fast radiative transfer model for assimilation of satellite radiance observations. *Quart.J.Roy.Meteor.Soc.*, **125**, 1407-1426.

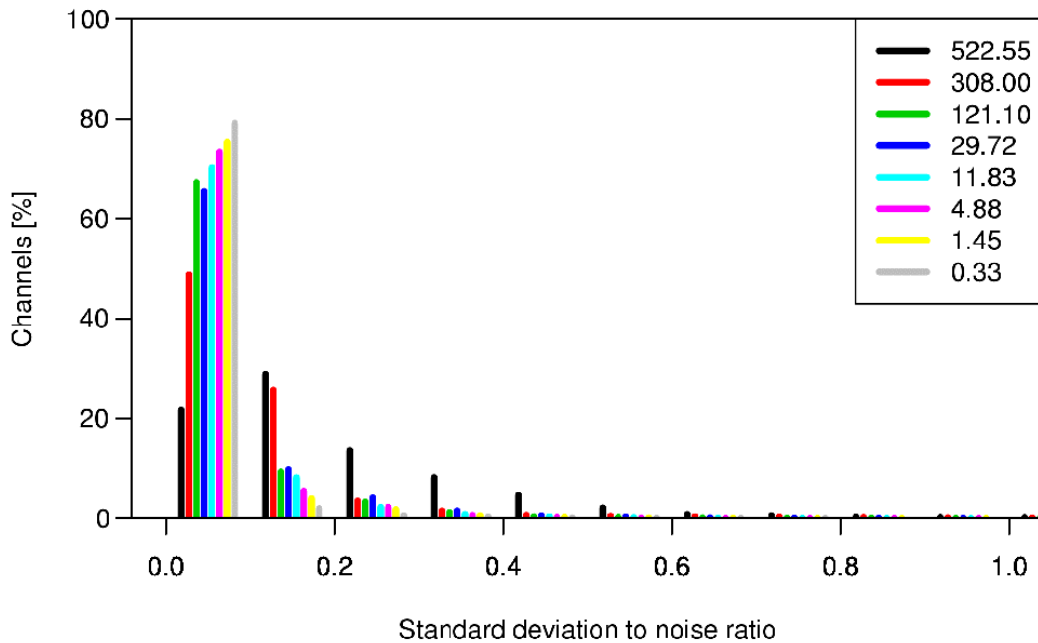


Figure 1: Distribution of the number of MIPAS channels [%] versus the standard deviation of the RTMIPAS-LBL radiance differences, scaled by the MIPAS noise. Results for 8 selected tangent pressures are shown, with tangent pressures [hPa] indicated in the legend.

High-Resolution Marine Wind Retrieval Using Synthetic Aperture Radar

Richard Danielson⁽¹⁾, Michael Dowd⁽¹⁾, Harold Ritchie^(1,2) and Luc Fillion⁽²⁾

⁽¹⁾Dalhousie University, Halifax NS, Canada

⁽²⁾Meteorological Research Branch, Dorval QC Canada

As weather prediction systems continue to encompass an increasing range of scales, there is a practical need to combine simulated fields with observations that are valid on these newly resolvable space and time scales. Surface wind fields over the ocean are highly variable on scales of a few kilometers and an accurate specification is important for a wide variety of applications. The high horizontal resolution of synthetic aperture radar (SAR) offers the potential for sub-kilometer winds and SAR measurements by RADARSAT-1 may be well suited for incorporation into a coastal data assimilation system. We explore the feasibility of combining SAR observations and high-resolution numerical simulations for coastal regions of eastern Canada. In the context of a variational data assimilation approach, we consider estimation of vector wind fields from SAR. The scalar radar cross-section measured by SAR is a function mainly of Bragg scattering from capillary waves, which in turn varies roughly with wind speed. Although some scenes contain boundary layer roll convection, which is a good indication of wind direction, such features are not always present and the retrieval of the wind field is often underdetermined.

A wind calibration specific to SAR has yet to be performed. If SAR wind errors could be quantified, this would constitute an initial step toward the assimilation of such data into coastal models. Simple estimates of these errors are derived here using a variational approach. Collocations of ship/buoy, model, and SAR data have been assembled using 272 SAR acquisitions in May to November 2004, and processed on a 1 km grid resolution. The ship and buoy observations have been used as the reference dataset. The model winds are from analyses using the 15 km operational regional model at the Canadian Meteorological Centre (CMC). The ship and buoy data have been visually inspected, and the SAR data have been masked over land, sea ice, along beam seams, and where winds are below 3 m/s or over 33 m/s. Buoy observations within 90 minutes of a SAR acquisition have been used. They have been adjusted to the 10 m level and are considered valid within 50 km. A total of 5667 ship/buoy-model-SAR collocations have been obtained.

As a result of the scatterometer wind calibration effort (e.g. Stoffelen 1998), a relationship (CMOD) between wind and backscatter is available. Bragg scattering from capillary waves varies with wind speed, wind direction, SAR beam angle, and other processes. The empirical relation used here is CMOD5 (Hersbach 2003). CMOD has been derived using ERS scatterometry data. ERS is vertically polarized, whereas RADARSAT-1 is horizontally polarized, so we employ a polarization correction (Vachon and Dobson 2000).

The desired surface wind field is a weighted combination of the SAR observations and model winds that minimized a cost function assuming Gaussian error structures. The

errors in the SAR backscatters and winds are chosen to best fit the ship/buoy winds. Given wind errors of 1.7 m/s, the best choice for SAR errors appears to be 1.5% of the backscatter (smaller than in Portabella et al. 2002).

The results support the Gaussian error distribution as assumed in the form of the cost function. The “retrieved versus observed” bias is significantly smaller than the “model versus observed” bias, so the incorporation of the SAR backscatter observations has improved the analysis when compared with the ship/buoy observations. Hence the use of SAR observations in a variational context appears to improve the surface wind analysis produced by the CMC system.

In situ observations are also erroneous (Stoffelen 1998) because they are not representative of large areas (i.e, they are point observations rather than spatial averages). In order to avoid pseudo-biases in SAR observations, all error types should be considered, that is, a SAR wind calibration is still required.

Acknowledgements

Funding for this research is being provided by the Canadian Space Agency. SAR data were obtained through the Integrated Satellite Tracking of Oil Polluters (ISTOP) Program and were provided by RADARSAT International (RSI). The Canadian Centre for Remote Sensing made available code to manipulate this data. Bridget Thomas of Environment Canada assisted with the vertical adjustment of the ship/buoy data.

References

- Hersbach, H., 2003: An improved geophysical model function for ERS C-band scatterometry. ECMWF technical memorandum 395 (available at www.ecmwf.int/publications).
- Portabella, M., A. Stoffelen and J.A. Johannessen, 2002: Toward an optimal inversion method for synthetic aperture radar wind retrieval. *J. Geophys. Res.*, **107** (C8), 3088. doi:10.1029/2001J000925.
- Stoffelen, A., 1998: Toward the true near-surface wind speed: Error modeling and calibration using triple collocation. *J. Geophys. Res.*, **103** (C4), 7755-7766.
- Vachon, P.W., and F.W. Dobson, 2000: Wind retrieval from RADARSAT SAR images: Selection of a suitable C-band HH polarization wind retrieval model. *Can. J. Remote Sens.*, **26**, 306-313.

Forward modelling of ground based GPS Slant Total Delay observations

Reima Eresmaa

Finnish Meteorological Institute

e-mail: reima.eresmaa@fmi.fi

1 Introduction

The NWP systems with horizontal resolutions near kilometric scales require high resolution observations. Microwave phase delays observed at geodetic Global Positioning System (GPS) receiver stations provide potential for exploitation in numerical humidity analysis (e.g. Bevis et al., 1992). The phase delay observations can be directly assimilated in the variational assimilation system of High Resolution Limited Area Model (HIRLAM 3D-Var; Gustafsson et al., 2001). Observation modelling by an observation operator is a necessary step in the variational assimilation.

2 Slant Total Delay observation operator

Modelling of a Slant Total Delay (STD) observation is complicated by the following aspects. First, the observation is dependent on refractivity N and thus on several model variables (pressure p , temperature T and specific humidity q). Second, the observed quantity is an integral of refractivity along the signal path. Third, the values of p , T and q need to be interpolated to the slanted signal path and not only to the vertical column at the observation location. However, the signal path is not known in advance. Therefore, signal path determination is an important task of the observation operator. Other tasks are projection of the model variables from the model grid to the signal path, calculation of refractivity as a function of the model variables, and integration of refractivity to produce STD.

The STD observation operator has been implemented in HIRLAM 3D-Var at the Finnish Meteorological Institute (FMI). In this observation operator, the signal path determination algorithm is based on the Line of Sight (LoS) -approximation. Thus, it uses the azimuth and zenith angles corresponding to the geometrical direction in which the broadcasting satellite is as viewed at the receiver. This direction is called here as the Direction of Geometry (DoG). Explicit corrections have been added on top of the simplest LoS -based model in order to account for zenith angle variations along the signal path.

3 Validation of the observation operator

The observation operator is validated by comparing the modelled STD with the observations. The STD observations used here are post-processed at the Technical University of Delft and they originate from 17 receiver stations in the Western Europe. STD is modelled using the operational HIRLAM of FMI with 0.2° horizontal resolution. The significance of each of the explicit corrections has been investigated by constructing five observation operator versions. These are summarized in Table 1.

The systematic part (bias) of the difference between modelled and observed STD is plotted in the upper panel of Fig. 1 as a function of the satellite zenith angle. The shaded region shows the number of observations in each 1° zenith angle bin. At the small zenith angles, i.e. when the satellite is close to the zenith direction, the bias is negative (the modelled STD is smaller than the observed). This is consistent with the biases of Zenith Total Delay (ZTD) observations reported by Gustafsson (2002). The bias at the large zenith angles is strongly sensitive to the forward modelling strategy. The most important single modelling improvement on top of LoS -approach is accounting for the effect of the curvature of the Earth.

Version	Characteristics
DoG	Uses Direction of Geometry
ITER	Like DoG, but the NWP model level height gradients included
CURV	Like DoG, but the effect of the curvature of the Earth included
BEND	Like DoG, but the effect of the refractive bending included
ADV	The effects of model level height gradients, curvature of the Earth and refractive bending included

Table 1: Observation operator versions used for comparison between modelled and observed STD.

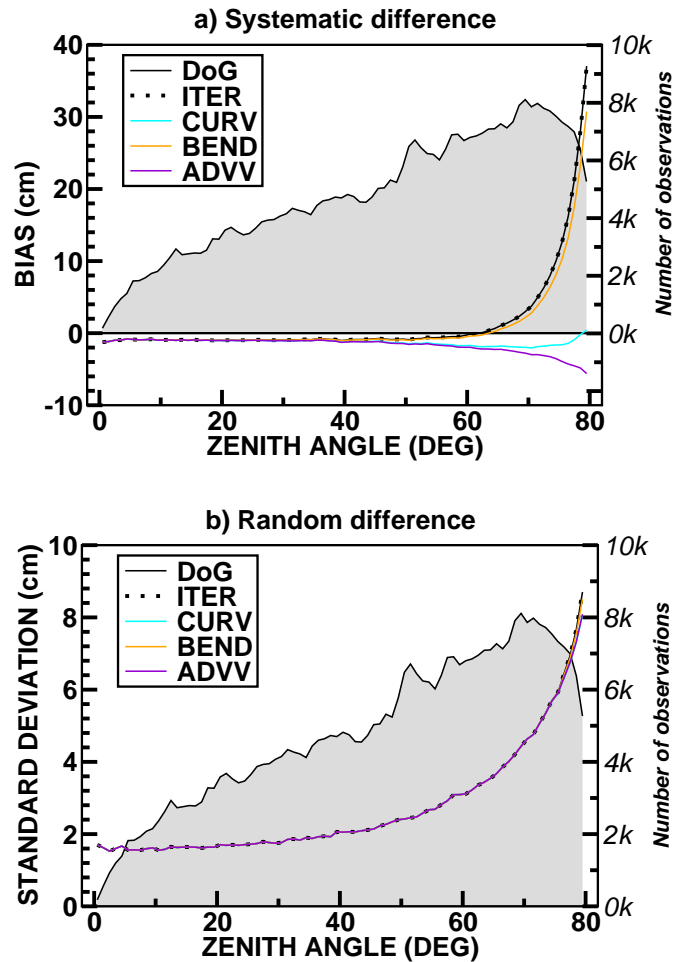


Figure 1: Systematic (upper) and random (lower) parts of the difference between modelled and observed STD as a function of satellite zenith angle.

The lower panel of Fig. 1 shows the random part (standard deviation) of the difference between modelled and observed STD. There is practically no difference between observation operator versions. This suggests that the signal paths as determined by one or the other observation operator version are fairly close to each other and therefore the model state differences along the different paths are negligible. Thus, it is concluded that the accuracy of the signal path determination algorithm seems to be sufficient for STD modelling.

References

Bevis, M, Businger, S, Herring, T, Rocken, C, Anthes, R and R Ware, 1992: GPS meteorology: Remote sensing of atmospheric water vapor using the Global Positioning System. *J. Geophys. Res.*, **97**, 15787–15801.

Gustafsson, N, 2002: Assimilation of ground-based GPS data in HIRLAM 3D-Var. Proceedings of the HIRLAM Workshop on Variational Data Assimilation and Remote Sensing, Finnish Meteorological Institute, Helsinki 21-23 Jan 2002. 89–96. Available from the HIRLAM Project, c/o Per Undén, SMHI, S-60176 Norrköping, Sweden.

Gustafsson, N, Berre, L, Hörnquist, S, Huang, X-Y, Lindskog, M, Navascués, B, Mogensen, K S and S Thorsteins-son, 2001: Three-dimensional variational data assimilation for a limited area model. Part I: General formulation and the background error constraint. *Tellus*, **53A**, 425–446.

Adaptive thinning of atmospheric observations in data assimilation with vector quantization and filtering methods – the first steps

Christoph Gebhardt¹, Tilo Ochotta², Dietmar Saupe², Werner Wergen¹

¹Deutscher Wetterdienst, ²Universität Konstanz, Fachbereich Informatik und Informationswissenschaft
christoph.gebhardt@dwd.de

An important task in data assimilation for numerical weather prediction is the effective exploitation of large amounts of data produced by current and future observation systems, in particular satellite instruments. The high spatial and temporal density of these data is on the one hand highly valuable for estimating an initial state in the numerical forecast process. But on the other hand such data sets significantly increase the computational costs of the assimilation and, moreover, can violate the assumption of spatially independent observation errors and more complex observation error statistics would be needed leading to additional increase in the computational costs.

Thinning approaches which effectively reduce the number of analyzed observations but at the same time retain as much of the essential information content as possible can help to overcome these problems. Liu & Rabier (2002) investigated assimilations of synthetic data with fixed spatial thinning intervals in a simplified model. They suggest that the optimal thinning which minimizes the analysis error depends on the spatial resolution of the model and of course on the degree of approximation of the observation error matrix with respect to its off-diagonal elements. The use of an ‘influence matrix’ of observations (Cardinali et al., 2003) is under investigation at ECMWF.

We develop thinning algorithms in an interdisciplinary project which are inspired by simplification methods from geometry processing in computer graphics and by clustering algorithms in vector quantization.

In a first method (‘estimation error method’), we iteratively estimate the redundancy of the current data set and remove the most redundant observation. The degree of redundancy of an observation is defined to be inversely proportional to the interpolation error of its reconstruction obtained by applying an interpolation filter to a neighborhood in which the observation is removed.

In a second scheme (‘cluster method’), the number of points in the output set is increased iteratively. These observations correspond to centers of clusters of observations. A distance measure that combines spatial distance with the difference in observation values defines an error measure for the overall quality of a clustering.

We apply the two methods to ATOVS satellite data which are processed in a 1D-Var scheme to retrieve profiles of atmospheric temperature and humidity. The profiles are again input data for the global analysis scheme of DWD.

Since the information gained by assimilating the data does not directly depend on the observations themselves but on their innovations to a first-guess state, we apply the thinning to the differences between bias-corrected observed brightness temperatures (TB_obs) and their first-guess (TB_FG, e.g. 3h-forecast temperatures transformed with RTTOV7) for those channels to be used in the 1D-Var scheme.

In a first test, we compared the two methods to a simple stepwise thinning which takes every third observation in zonal and meridional direction (*Figure 1*). For identical numbers of observations, the cluster method is spatially more homogeneous as the stepwise method which has the highest data density close to nadir view. The estimation error method leads to a more patchy thinning because it does not take into account the spatial distance as explicitly as the cluster method.

Figure 2 compares the three methods in terms of data density per 10.000km^2 . The difference maps show that both cluster and estimation error method tend to increase the density compared to the stepwise thinning at the edges along the satellite track. This effect is more pronounced in the cluster method. In the region of overlapping tracks off the shore of southern Argentina with differing TB_obs-TB_FG due to time differences, the estimation error method results in the highest density of all methods. The thinning by the estimation error method is generally weaker in regions with more variable data because each observation in such an area is less likely to be redundant referring to its neighbors leading to small regions of comparably high data density. The cluster method also tends to retain more data in such regions but to a lesser degree due to its spatial constraint and the definition of a cluster center as some kind of balancing representative of its neighborhood. The histogram of data densities for 3387 observations confirms these effects. Compared to the stepwise thinning, the two other methods shift data density to higher values but significantly only up to 1 observation/ 10.000 km^2 for the cluster method but more effective for the estimation error approach. A density value for a distribution of 3378 points which is homogeneous over the area covered by the tracks can be approximated by 0.65 obs./ 10.000 km^2 which is close to the maximum of all methods in the histogram.

Tests with thinning down to lower numbers of retained observations reveal that the estimation error method tends to increase the variance of the innovation statistics. Consequently, thinning down to small data sets bears the danger of overemphasizing the extremes of TB_obs-TB_FG which on the one hand are possibly of most value in updating the first-guess but on the other hand are most affected by deficiencies of the preceding quality control of the data.

Although these first test results help to figure out the properties of the methods, the proper choice of method, degree of thinning, and parameters has to be determined in a complete assimilation and forecast experiment which is ongoing work.

Liu, Z.-Q. and Rabier, F. (2002): The interaction between model resolution, observation resolution and observation density in data assimilation: A one-dimensional study. *Q.J.R. Meteorol. Soc.*, **128**, pp.1267-1386.

Cardinali, C., Pezzulli, S. and Andersson, E. (2003): Influence matrix diagnostic of a data assimilation system. *ECMWF Seminar 'Recent developments in data assimilation for atmosphere and ocean'*, 8-13 September 2003.

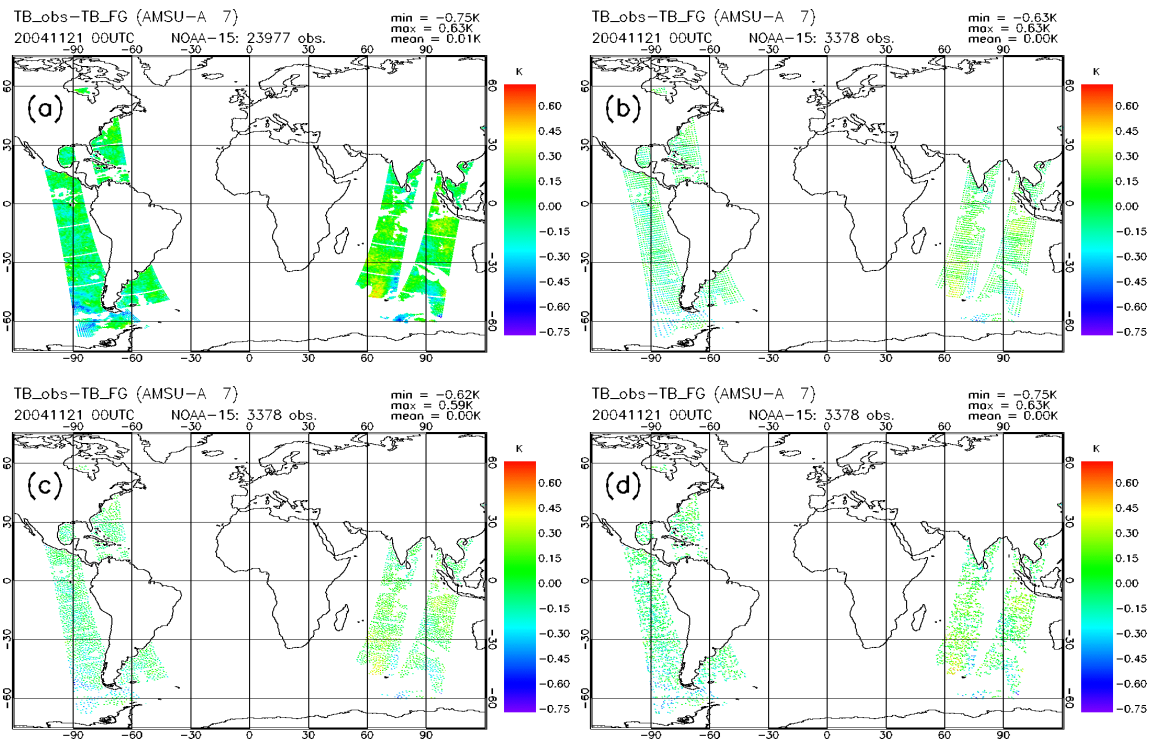


Figure 1: Bias-corrected minus first-guess brightness temperatures for channel AMSUA-A 7 of NOAA-15 on 21st Nov 2004 00 UTC for (a) unthinned data and after thinning by (b) stepwise, (c) cluster, and (d) estimation error method.

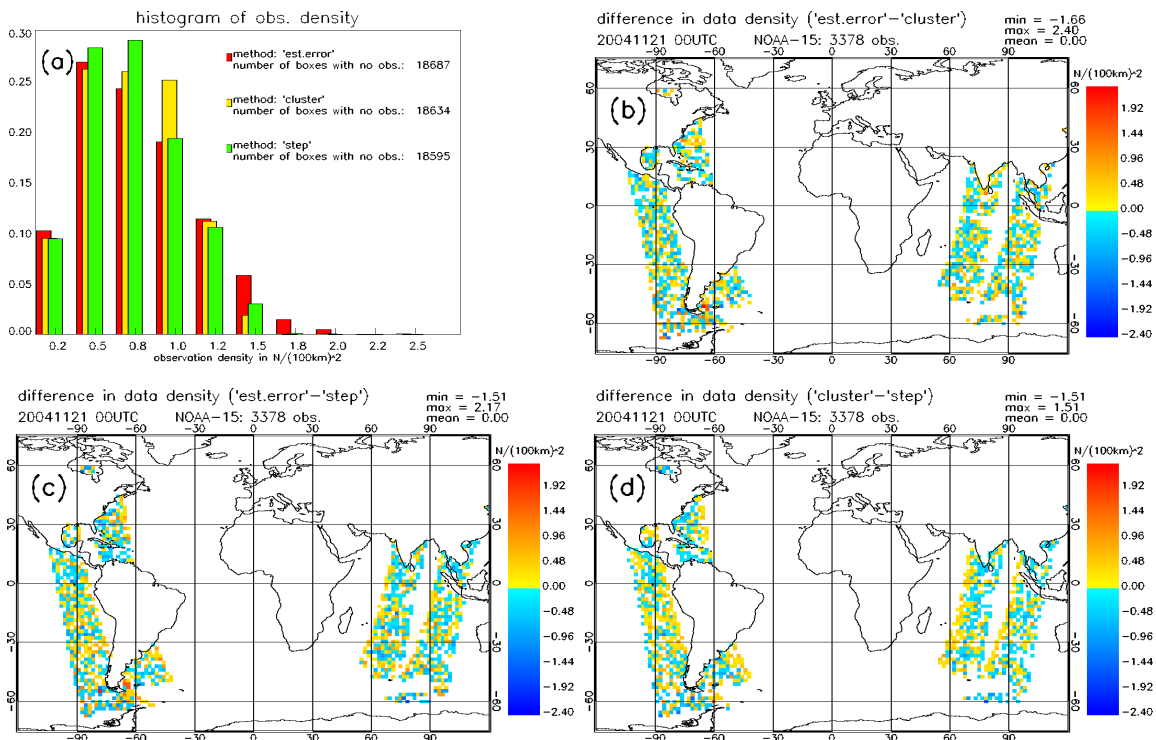


Figure 2: (a) histogram of data density after thinning with each method down to 3378 observations and difference maps of data density for (b) estimation error minus cluster, (c) estimation error minus stepwise, and (d) cluster minus stepwise method.

Assimilation of new sounder data in the operational system at Météo-France

Elisabeth Gérard, Thibaut Montmerle* and Florence Rabier

CNRM/GMAP, Météo-France, Toulouse

*: EUMETSAT fellow

email: elisabeth.gerard@meteo.fr

Since October 2004, new data from the ATOVS sounders on board the NOAA satellites have been assimilated in the Arpege model. Let us recall that the ATOVS sounder includes 3 instruments (AMSU-A, AMSU-B et HIRS). Until now, data from the AMSU-A and HIRS instruments that were assimilated, provided information on atmospheric temperature and humidity profiles. The additional use of AMSU-B data has been tested in 2004, with a significant positive impact in terms of geopotential forecast scores, and major changes in the humidity analysis over the continent. One drawback of the ATOVS data, is that they are received by NOAA in the United-States, then transmitted to Europe. This implies delays to the reception of data used in the Arpege "production" analyses used to initialise the forecast model, knowing the tight schedule imparted. A complement to the processing of these global data is to use data processed locally in local reception stations, and then redistributed by EUMETSAT in a much shorter time (the so-called EARS project). These observations are tailored for our needs by CMS, where reconstructed long orbits guarantee a better data homogeneity, as shown in Figure 1. This processing allows more data to be inserted by the "production" analyses, and also in the "assimilation cycle" analyses providing the best atmospheric description in near real time, as can be seen in Figure 2. Due to these changes, data from the ATOVS sounders are currently fully used in operations, and the focus will now be on new sounders, such as the advanced AIRS sounder from NASA and the IASI interferometer soon onboard the Metop satellite (CNES/EUMETSAT).

ATOVS= Advanced TIROS Operational Vertical Sounder

NOAA= National Oceanic and Atmospheric Administration

AMSU= Advanced Microwave Sounding Unit

HIRS= High Resolution Infrared Radiation Sounder

EARS= EUMETSAT ATOVS Retransmission Service

AIRS= Atmospheric Infra-Red Sounder

IASI= Interféromètre Atmosphérique de Sondage dans l'Infrarouge

= Infrared Atmospheric Sounding Interferometer

CMS=Centre de Météorologie Spatiale, Météo-France, Lannion.

NOAA-16 I1c AMSU-B 1
 2004-03-24 09:20 2004-03-24 14:38
 Orbits 18058-18061

HRPT stations : lannion

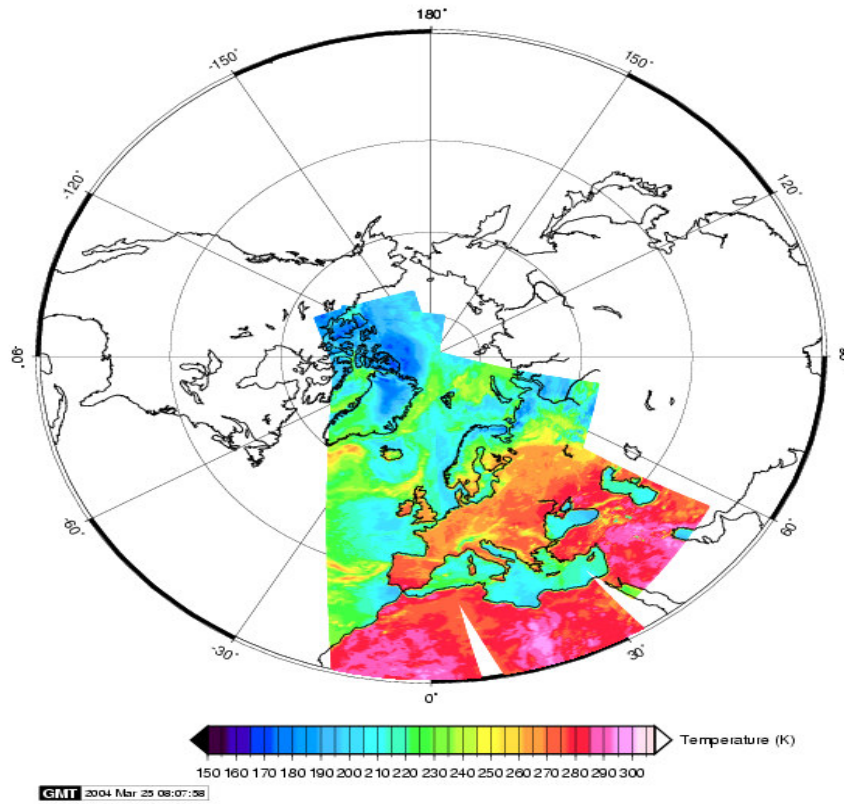


Figure 1: Data distribution for the ATOVS data created by CMS (Lannion) from EARS and locally received data.

1 er mai 2004 r12

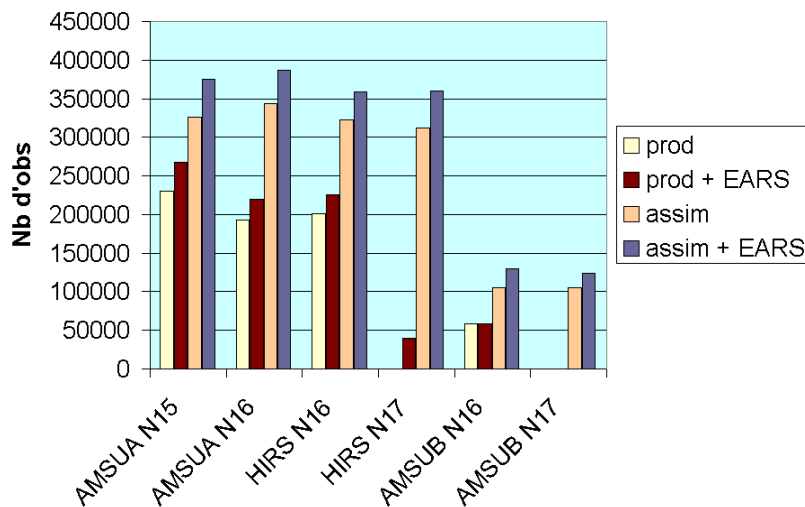


Figure 2: Number of observations available for the various 20040501, 12Z analyses.

Initialization Scheme for Water Substances in the operational NHM

Jun-ichi Ishida* and Kazuo Saito**

*Numerical prediction Division, Japan Meteorological Agency, Tokyo, Japan

**Forecast Research Department, Meteorological Research Institute, Tsukuba, Japan

E-mail: j_ishida@met.kishou.go.jp, ksaito@mri-jma.go.jp

The Japan Meteorological Agency (JMA) started the operational run of a nonhydrostatic model (NHM) on 1 September 2004 in place of the MSM (the former operational mesoscale model of JMA). NHM was developed based on the Meteorological Research Institute/Numerical Prediction Division unified nonhydrostatic model (Saito et al., 2001).

The bulk cloud microphysics used in NHM contains prognostic variables for the mixing ratios of water vapor, cloud water, rain, cloud ice, snow, and graupel. The JMA Meso 4D-VAR (Ishikawa and Koizumi, 2002) which gives the initial fields of NHM does not produce the initial fields for these water substances except the water vapor. Since the initial values of these water substances were set to zero at the early stage of development of NHM, a spin-up problem had been clearly seen where the precipitation is underestimated at initial time (Ishida and Narita, 2003). We have developed a new initialization scheme for the water substances.

Since the operational NHM is run four times a day, a 6-hourly forecast-forecast cycle system is employed for the water substances. The mixing ratios of cloud water, rain, cloud ice, snow, and graupel from output of the preceding (6 hours before) forecast are used as first guess values. These guess values are set to zero at the grid point where the relative humidity given by the Meso 4D-VAR analysis is less than 90 per cent in consideration of the consistency with the analysis field.

Figure 1 shows the one hour precipitation of the first three hours initialized at 06 UTC 30 October 2004. The left column indicates the observation by the Radar-AMeDAS analysis. The middle and right columns show the forecasts by NHM without and with initialization of water substances, respectively. It is clear that precipitation of NHM without initialization is much less than that of observation. Figure 2 shows the time sequence of numbers of grid points exceeding threshold values of precipitation by the Radar-AMeDAS analysis (red), by NHM with initialization (green), and by NHM without initialization (blue). The grid points over land and over sea within 100 km from the coast are counted (the area is wider than that of Fig. 1). The underestimation of precipitation in NHM without initialization is significant at the first one hour, and continues until three or four hours for weak rain (threshold: 0.5mm/hr) and six hours for moderate rain (threshold: 2mm/hr). The initialization scheme significantly improves this underestimation. Figure 3 shows the bias and threat scores of NHM with and without initialization and MSM for eight cases from 18 July to 19 July 2003. The bias scores of NHM with initialization are quite improved and the threat scores are also increased. The scores for longer periods and detailed validation of the operational NHM are described in Saito et al. (2005).

The initialization scheme of NHM for water substances has improved the precipitation forecast at the beginning of the forecast. Although the goal of initialization of water substances is a 4D-VAR analysis using bulk cloud microphysics, this scheme has been adopted into the operational NHM because of its effectiveness and simplicity. Since the current scheme does not consider the observational data of rainfall, a new additional treatment for initialization using observed rainfall is under development.

References.

- Ishida, J. and M. Narita, 2003: Verifications, *Separate volume of annual report of NPD*, **49**, 93-106. (in Japanese)
- Ishikawa, Y. and K. Koizumi, 2002: One month cycle experiments of the JMA mesoscale 4-dimensional variational data assimilation (4D-Var) system. *CAS/JSC WGNE Res. Act. in Atmos. and Ocea. Modelling.*, **32**, 0126-0127.
- Saito, K., T. Fujita, Y. Yamada, J. Ishida, Y. Kumagai, K. Aranami, S. Ohmori, R. Nagasawa, S. Tanaka, C. Muroi, T. Kato and H. Eito, 2005: The operational JMA Nonhydrostatic Mesoscale Model. *Mon. Wea. Rev.* (to be submitted)
- Saito, K., T. Kato, H. Eito and C. Muroi, 2001: Documentation of the Meteorological Research Institute/Numerical Prediction Division unified nonhydrostatic model. *Tec. Rep. MRI*, **42**, 133pp.

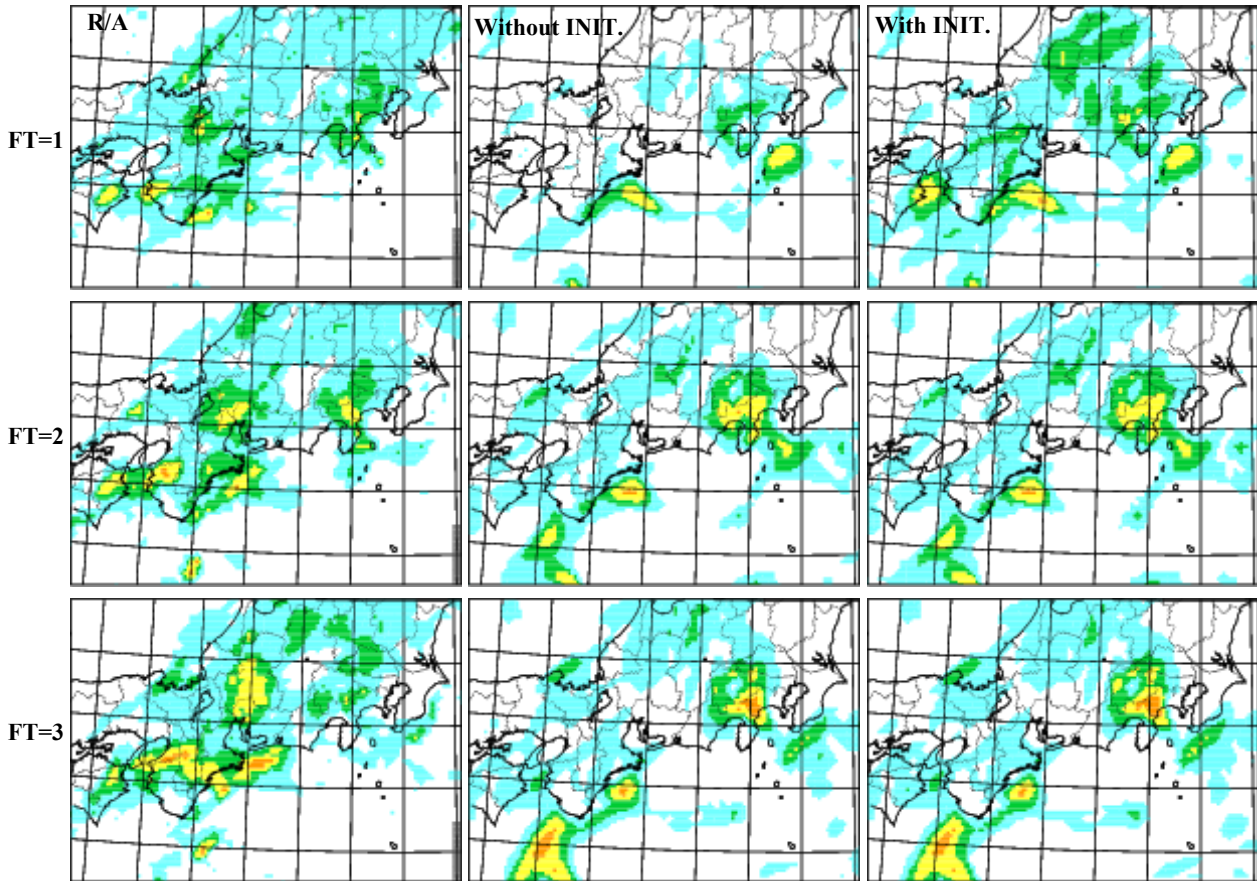


Fig.1. One hour precipitation. Left: observed by Radar-AMeDAS analysis. Center: forecasted by NHM without initialization. Right: forecasted by NHM with initialization. The initial time of NHM is 0600 UTC 30 October 2004.

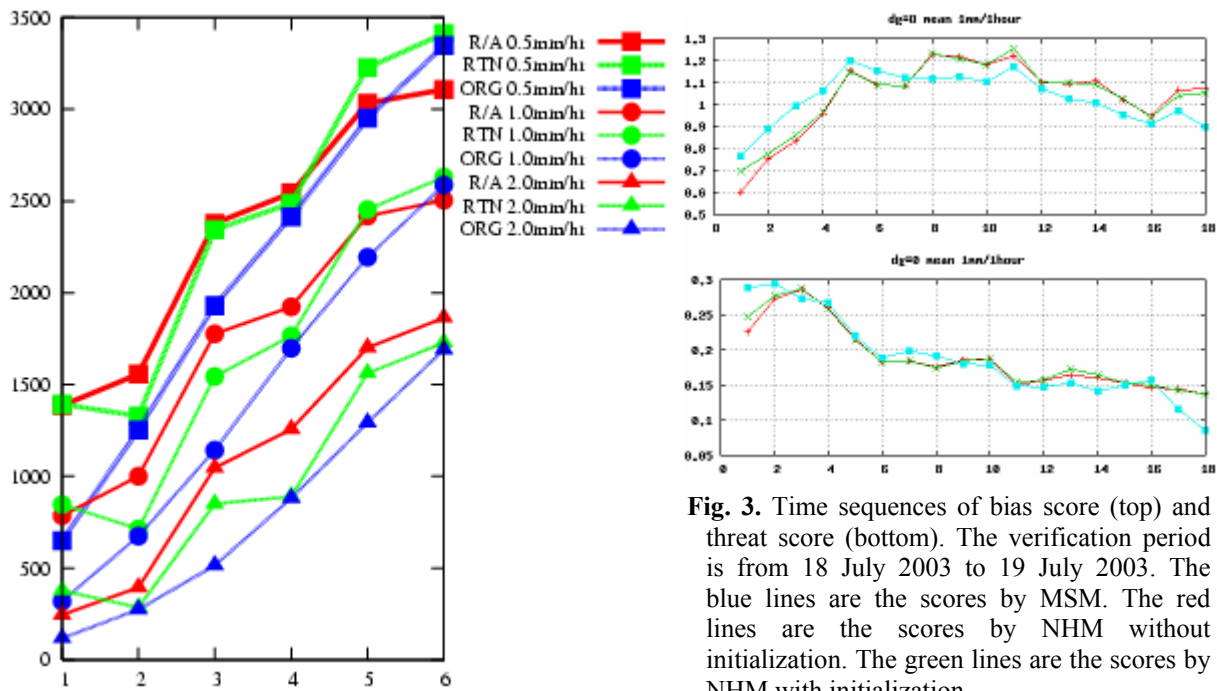


Fig. 2. Time sequence of numbers of grid points exceeding threshold values of precipitation. Red: Radar-AMeDAS analysis. Green: NHM with initialization. Blue: NHM without initialization.

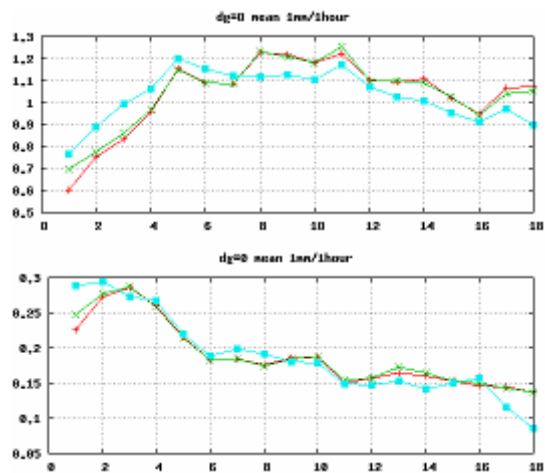


Fig. 3. Time sequences of bias score (top) and threat score (bottom). The verification period is from 18 July 2003 to 19 July 2003. The blue lines are the scores by MSM. The red lines are the scores by NHM without initialization. The green lines are the scores by NHM with initialization.

A 4-dimensional variational assimilation system for the JMA Global Spectrum Model

Takashi Kadowaki

Numerical Prediction Division, Japan Meteorological Agency
1-3-4 Otemachi, Chiyoda-ku, Tokyo 100-8122, JAPAN

email: tkadowak@naps.kishou.go.jp

The JMA has been developing a 4-dimensional variational data assimilation (4D-Var) system for the Global Spectrum Model(GSM). An incremental approach is taken to save computational time. The method calculates an analysis increment at a low resolution (T63L40) and then adds the increment to the high-resolution first guess(TL319L40). The model for forecast uses the semi-Lagrangian scheme(Yoshimura et al., 2003). The tangent-linear and adjoint model uses the Eulerian scheme with simplified physics. Assimilated observational data are the same as in the operational 3D-Var system. Two typhoon bogus methods are applied. In the analysis for the assimilation cycle, typhoon bogus profiles are embedded in first guess fields of surface pressure, temperature, and wind in the same way as in the 3D-Var. In the analysis for the model forecasts, pseudo observational data of sea-surface pressure and wind around a typhoon center are assimilated together with other observational data.

In order to evaluate the system performance, forecast-analysis cycle experiments were performed for each of one-month periods of January and August 2004. Nine-day forecasts were made once a day from 12 UTC initial conditions throughout the experiment periods. Figure.1 shows the RMSE of 500hPa geopotential height against the initialized analysis for January and August cases. The forecasts starting from 4D-Var are better than those from 3D-Var in the January case. In the August case, the forecasts starting from 4D-Var are better than those from 3D-Var in Southern Hemisphere and almost neutral in Northern Hemisphere. Figure.2 shows the RMSE and BIAS of 850hPa temperature against radio-sonde observations in the tropical region for the August case. The RMSE for 4D-Var is generally better than that for 3D-Var. The BIAS for 4D-Var is worse than that for 3D-Var in short-range forecasts, and it may result from model-originated cooling bias in the lower troposphere. Figure.3 shows the track-forecast error for typhoons T0411- T0419. The typhoon track-forecast error is reduced compared to 3D-Var except for very short-range forecasts.

This 4D-Var system will be operational in early 2005.

References:

Yoshimura, H., T. Matsumura, 2003: A Semi-Lagrangian Scheme Conservative in the Vertical Direction. Research Activities in Atmospheric and Ocean Modeling, CAS/JSC Working Group on Numerical Experimentation, 33, 0319-0320.

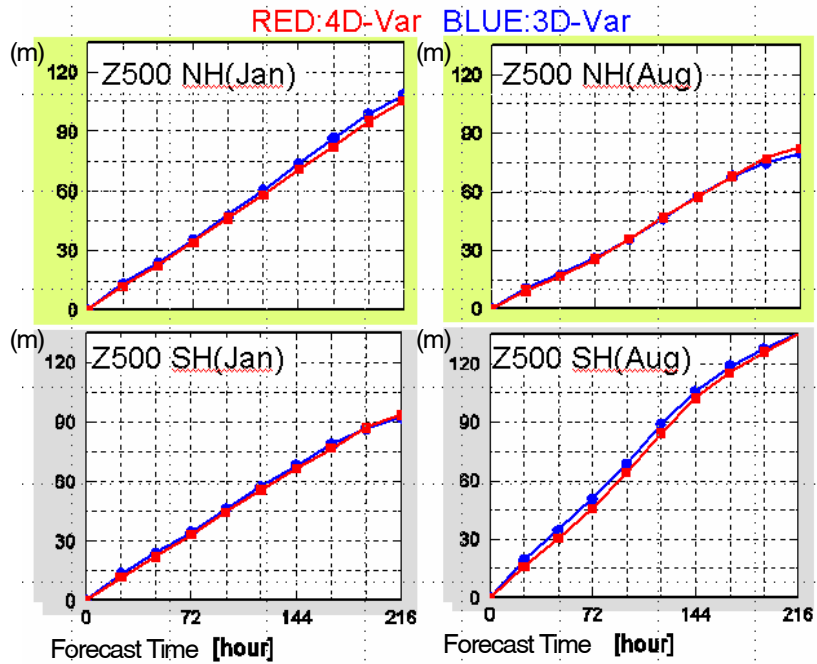


Fig.1 RMSE of 500hPa geopotential height against the initialized analysis.

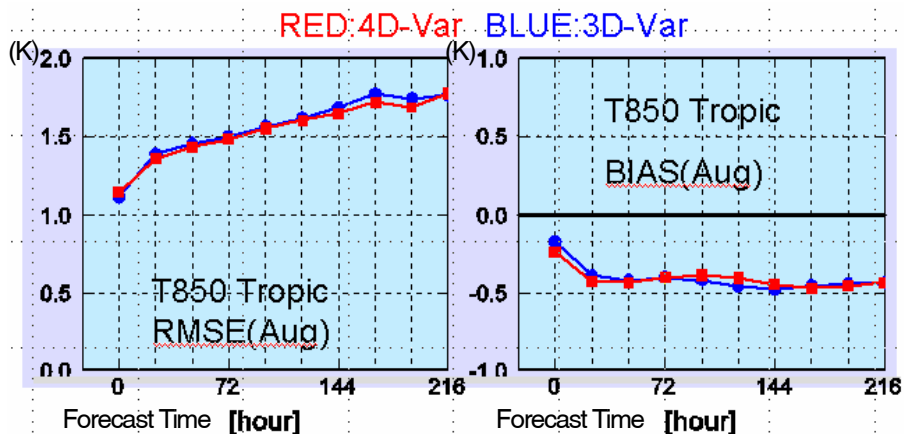


Fig.2 RMSE and BIAS of 850hPa temperature against radio-sonde observations.

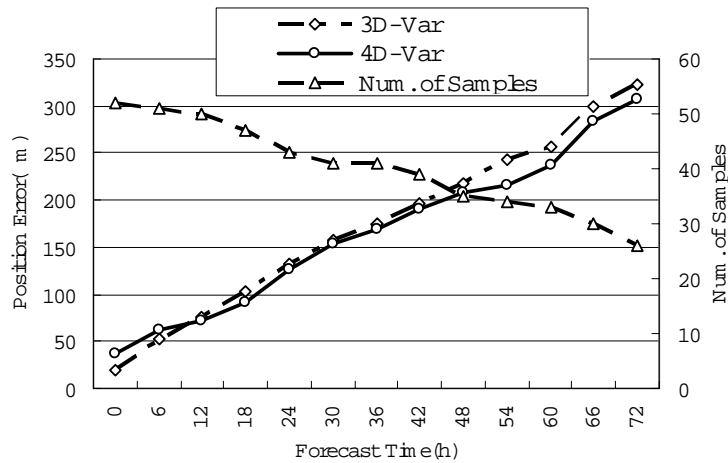


Fig.3 Position error of typhoon forecasts(T0411-T0419).

A cloud resolving 4DVAR data assimilation system based on the JMA non-hydrostatic model

Takuya KAWABATA^{1a}, Hiromu SEKO^a, Tohru KURODA^d, Yasutaka WAKATSUKI^c, Yuki HONDA^b,
Kyuichiro TAMIYA^a, Kazumasa AONASHI^a, Yoshinori SHOJI^a, Kazuo SAITO^a, Tadasi TSUYUKI^b

^aForecast Research Department of Meteorological Research Institute / JMA,

^bNumerical Prediction Division of Japan Meteorological Agency

^cAdvanced Earth Science and Technology Organization

^dMeteorological Research Institute / JST Cooperative System for Supporting priority Research

1. Introduction

Since April 2002, the Forecast Research Department of the Meteorological Research Institute (MRI) and the Numerical Prediction Division of Japan Meteorological Agency (JMA) have been developing a 4DVAR system based on the JMA non-hydrostatic model. MRI develops the system with a horizontal resolution less than 2 km to apply to the convective cloud systems. Because JMA-NHM adopts fully compressible non-hydrostatic equations and cloud microphysics, this cloud resolving assimilation system is expected to reproduce structures of convective cells in rainfall systems. A prototype of 4DVAR system that includes dry dynamics was developed (Honda et al. 2003). This system has been further developed to include the advection of water vapor (Kawabata et al., 2004). In this paper, this cloud resolving 4DVAR system is explained, and then the results of assimilation experiments using GPS-derived precipitable water vapor (PWV) and the radial wind observed by Doppler radars (RW) are introduced.

2. Background error

Our target scale is 2 km horizontal resolution and 1-hour assimilation window. We discuss the difference of background errors between 2km model and 5km model. The statistics of background error were obtained by NMC method (Parrish et al., 1992). Namely, we performed several runs of JMA-NHM with horizontal resolutions of 2 km and 5km, and then, calculated the statistics of background error. The time lags of the initial fields in 2 km model and 5 km model were set to 1 hour and 6 hour, respectively.

Figure 1 shows the horizontal correlation between east-west component of horizontal wind and pressure. We can see the geostrophic balance modes in the correlation of 5 km error. On the other hand, there is not any balance mode in 2km error. We can see some correlation mode in 2km error, but its scale is very different from the geostrophic balance mode in 5km error. These results indicate that 2km errors mainly include the scale of the meso convective rainfall system and 5 km error also include the synoptic scale feature.

3. Assimilation experiment

Our purpose of the development of this assimilation system is to investigate the mesoscale convective rainfall system and to forecast the heavy rainfall. As the target for data assimilation experiments of this study, the small thunderstorm, which generated over the Tokyo and developed into heavy rainfall, was adopted. Generally, the convections are generated by the low-level convergence of humid airflow. Thus, PWV and RW, which have information of water vapor and the low-level convergence, are expected to improve the forecast of heavy rainfalls. In this study, GPS-derived PWV and RW of Doppler radars were used as assimilation data.

3.1. Experiment design

To reproduce the generation of the thunderstorm, the horizontal interval of 2km was adopted and then the horizontal domain of the assimilation was set to be 44km x 44km to cover the convergence zone. Because the thunderstorm began to be generated at 06UTC, the assimilation window from 0600UTC to 0620UTC was adopted. We assimilated the GPS PWV at every 5 minutes and RW at every 1 minute.

3.2. Assimilation result

Figure 2 shows the observed horizontal wind field by dual Doppler radars, at 1km level. The thunderstorm indicated by the black square was developed into the heavy rainfall. In the precipitation region of the thunderstorm, the southerly flow converged with the northerly flow in the precipitation area.

¹ e-mail : tkawabat@mri-jma.go.jp

Figure 3 shows the first guess field and the analyzed field of horizontal wind and precipitable water vapor. In the guess field, southwesterly flow converged with weak southwesterly flow. When the GPS PWV and RW were assimilated, wind direction of the northern part of the domain was changed from southwesterly to northerly. Namely, the analyzed wind distribution became similar to observed one. For this change, the convergence of horizontal wind was more intensified than that of guess field. The intense convergence was maintained during the assimilation window. The convergence of water vapor was also stronger in the analyzed filed.

4. Future plan

We are to improve this system to assimilate the radar data and to investigate the mesoscale rainfall system or heavy rainfall. For this purpose, we are going to write tangent linear codes and adjoint codes of cloud microphysics.

References

1. Honda, Y., T. Kawabata, K. Tamiya, K. Aonashi, T. Tsuyuki and K. Koizumi, "Development of a 4DVAR data assimilation system ad JMA"(in Japanese), Preprints. 5th Workshop on the Nonhydrostatic Model, 2003
2. Kawabata, T., T. Kuroda, Y. Honda, K. Tamiya, K. Aonashi, T. Tsuyuki, and K. Koizumi, "A 4DVAR data assimilation system for the JMA Nonhydrostatic model to assimilate water vapor data" (in Japanese), Preprints. Spring meeting of Meteorological Society of Japan, 2004
3. Saito, K., T. Kato, H. Eito, and C. Muroi, "Documentation of the Meteorological Research Institute / Numerical Prediction Division Unified Nonhydrostatic Model", TECHNICAL REPORTS OF THE METEOROLOGICAL RESEARCH INSTITUTE, Vol. 42, 1-133, 2001
4. Seko, H., T. Kawabata, T. Tsuyuki, H. Nakamura, K. Koizumi, and T. Iwabuchi, "Impacts of GPS-derived Water Vapor and Radial Wind Measured by Doppler Radar on Numerical Prediction of Precipitation", Journal of the Meteorological Society of Japan, Vol. 82 No. 1B, 473-489, 2004b
5. Shoji, Y., H. Nakamura, T. Iwabuchi, K. Aonashi, H. Seko, K. Mishima, A. Itagaki, R. Ichikawa, and R. Ohtani, "Observation Improvement in GPS Analysis of Slant Path Delay by Stacking OneWay Postfit Phase Residuals", Journal of the Meteorological Society of Japan, Vol. 82 No. 1B, 301-314, 2004
6. Parrich, D.F, and J. C. Derber, "The National Meteorological Center's spectral statistical-interpolation analysis system", Monthly Weather Review, 120, 1747-1763, 1992

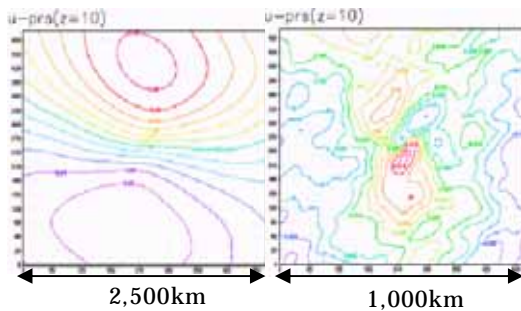


Fig. 1. Horizontal correlations between east-west component of horizontal wind and pressure. Left and right panels show 5km error and 2km error. Domain sizes of 5km and 2km error are 25000 km and 1000km, respectively.

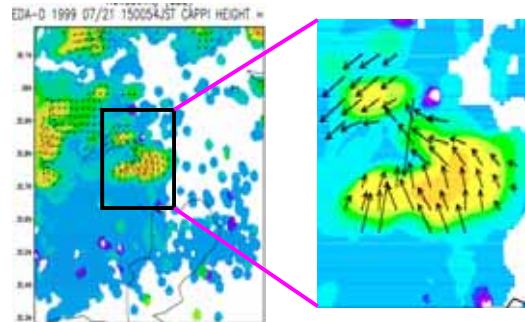


Fig.2. Observed horizontal wind field by dual Doppler radars, at the height of 1km . Right panel shows an enlarged area near the assimilation area.

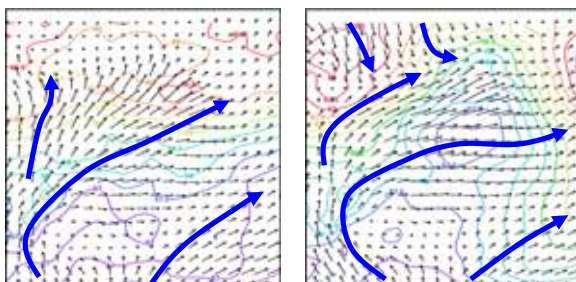


Fig. 3. First guess field (left) and analyzed field (right) at 0600 (UTC) 21 July 1999. Arrows and contour lines indicate horizontal wind and PWV at 1000 m.

Assimilation of ATOVS level-1c radiance data at JMA

Masahiro Kazumori, Kazuyo Fukuda, Hiromi Owada
Numerical Prediction Division, Japan Meteorological Agency
1-3-4 Otemachi, Chiyoda-ku, Tokyo 100-8122, JAPAN

email: kazumori@met.kishou.go.jp, kazuyo@naps.kishou.go.jp, howada@naps.kishou.go.jp

Since 28 May 2003, JMA has been used NOAA/NESDIS pre-processed radiances data (level-1d) in the ATOVS radiance assimilation system (Kazumori et al. 2003). The AAPP (ATOVS and AVHRR Processing Package) software was introduced to the JMA numerical weather prediction system on 25 August 2004. The ATOVS level-1b data from NOAA/NESDIS and the direct broadcast ATOVS data received at the Meteorological Satellite Center of JMA are pre-processed routinely and converted to the level-1c radiance data.

A new system for the ATOVS level-1c data assimilation was developed and RTTOV-7 (Saunders et al. 2002) was introduced as the radiative transfer model for the assimilation. In the system, the 1D-Var pre-process step and the 3D-Var analysis have been modified to deal with each instruments as an independent source of radiance data and these data are assimilated on its original scan geometry. Several pre-processing procedures in the 1D-Var step were improved. A horizontal thinning procedure was improved for three-satellite usage and new criteria for clear/cloud/rain conditions were defined for the level-1c data. A retrieval algorithm of cloud liquid water was introduced for the AMSU-A cloud detection. The removal of rain data based on the AAPP pre-process procedures was installed. Moreover, a new bias correction scheme for level-1c radiance was developed (Kazumori et al. 2004).

Preliminary observation system experiments were carried out with the T213L40 operational resolution of Global Spectral Model by using the radiance data of ATOVS (AMSU-A and AMSU-B) of NOAA15, NOAA16 and NOAA17 instead of current NESDIS pre-processed radiance data. The results of the experiment demonstrated large positive impacts on 500hPa geopotential height (Figure 1). And improvements of analysis field and forecast field are confirmed against radio-sonde observation for temperature and geopotential height (not shown). The new system was implemented on 2 December 2004.

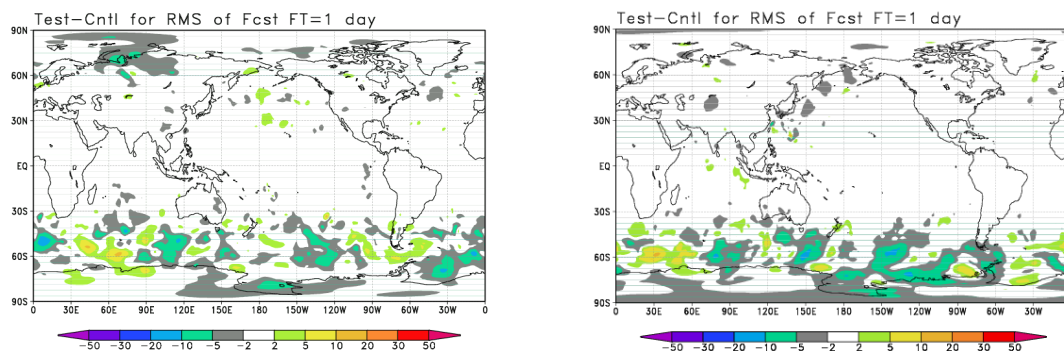


Figure 1. Differences of the averaged Root Mean Square forecast error for the 500-hPa geopotential height between the TEST and CNTL at one day forecast for the January 2004 (left) and August 2004(right). They are produced by the forecasts verified against their own initial conditions during 31 day period from 1 to 31 January 2004, and during 31 day period from 1 to 31 August 2004, respectively. The negative value indicates smaller errors in the TEST run.

Reference

- Kazumori, M., K. Okamoto, and H. Owada, 2003: Operational use of ATOVS radiances in global data assimilation at the JMA, Proceedings of 13th International TOVS International TOVS Study Conference, 37-42.
- Kazumori, M., K. Okamoto, and H. Owada, 2004: Improvements of ATOVS radiance-bias correction schemes at JMA, CAS/JSC WGNE Res.Act. Atmos. Ocea. Modelling, 01-20 01-21
- Saunders, R., E. Andersson, P. Brunel, F. Chevallier, G. Deblonde, S. English, M. Matricardi, P. Rayner, and V. Sherlock, 2002: RTTOV-7 Science and validation report.

MODIS polar winds assimilation at JMA

Masahiro Kazumori, Yoshiyuki Nakamura
Numerical Prediction Division, Japan Meteorological Agency
1-3-4 Otemachi, Chiyoda-ku, Tokyo 100-8122, JAPAN
email: kazumori@met.kishou.go.jp, nakamura-y@met.kishou.go.jp

Introduction

The geostationary satellites have provided wind data from the tropics to mid-latitudes for global numerical weather prediction (NWP), and their atmospheric motion vectors play a significant role to grasp the structure of wind field on global scale. While the polar regions have been remained as data poor regions for long time because the observations at high latitudes are difficult for the geostationary satellites. Furthermore, radiosonde and aircraft observations are sparse in the polar regions.

The MODIS is an instrument carried on the Terra and Aqua polar-orbiting satellites. Recently, the MODIS polar winds are derived at Cooperative Institute for Meteorological Satellite Studies (CIMSS) by tracking structures in successive swaths from the MODIS instruments (Key et al. 2003). Cloud patterns are tracked in the Infrared band and water vapour features are tracked in 6.7 μ m band.

Aiming to improve the forecast skill of NWP, JMA has started the acquisition of the MODIS polar winds from CIMSS since July 2003 and has investigated the quality of the MODIS polar winds.

Observation system experiments

The MODIS polar winds were acquired from a CIMSS FTP server via Internet. The earliest cut off time is 440 minutes for the cycle analyses, and 150 minutes for the early analyses at JMA. 80% of the produced data are available for the cycle analyses. The statistical investigation revealed that the MODIS polar winds in the Antarctic have larger BIAS against the first guess than those in the Arctic (Figure 1). And the lower level MODIS polar winds have poor quality. The quality of the MODIS polar winds in the Northern Hemisphere was acceptable for assimilation.

The MODIS polar winds assimilation experiments were performed for July 2003 and January 2004 with the JMA Global Spectral Model (GSM). In the experiments, the MODIS polar winds were used in the Arctic. The MODIS polar winds complement other observations and introduce analysis increment in data sparse regions. And by using the data from the couple of satellites, a better spatial coverage was acquired than single satellite case.

Analysis impacts of the MODIS polar winds were restricted in the Arctic. Increase in 500hPa geopotential height over ocean and decrease over land were found for both July 2003 and January 2004 (not shown).

As for forecast impacts, large improvements in forecast scores of geopotential height (Figure 2) and wind fields were found at 500hPa. The MODIS polar winds revealed that the analysis in the polar region is extremely important for the forecast of mid-latitudes because the improvements in the polar region at the initial state spread to mid-latitudes with the procession of forecasts.

Summary

The MODIS polar winds assimilation experiments were performed for July 2003 and January 2004 with the JMA GSM. Because the experiments showed the positive impacts on forecast scores, JMA started the operational assimilation of Terra and Aqua MODIS polar winds in the Arctic on 27 May 2004. And the quality of the MODIS polar winds in the Antarctic has been better since July 2004, the use of the MODIS polar winds in the Antarctic was started on 16 September 2004.

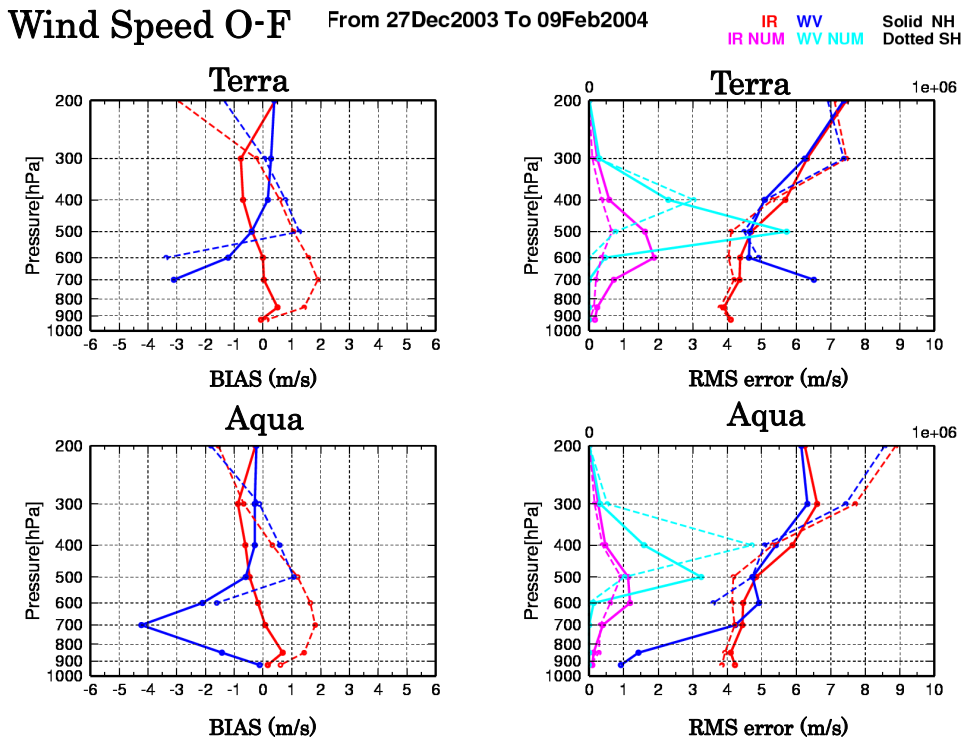


Figure 1. Statistics of wind speed against first guess for all MODIS polar winds from the CNTL. The upper panels are for Terra MODIS and lower ones for Aqua MODIS. Left panels show BIAS and right for the RMS error. Red line is for IR winds and blue line for WV winds. Solid lines are for the Arctic and dotted lines for the Antarctic. Light colour lines in the right panels show the numbers of data. The period is from 27 December 2003 to 9 February 2004.

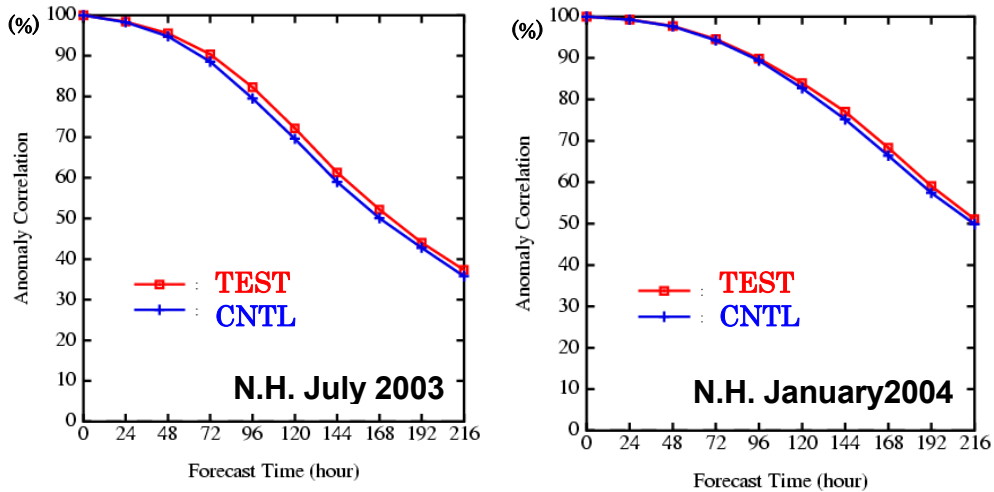


Figure 2. Anomaly correlation as a function of forecast time for the 500hPa geopotential height forecast in the Northern Hemisphere. Left panel shows that of July 2003 and right panel shows that of January 2004. The TEST (red) and the CNTL (blue) have been verified against their own analysis. The period is July 1-31, 2003 and January 1-31, 2004, respectively. The Northern Hemisphere is defined as the area north of 20 degrees.

Reference

Key, J. R., D. Santek, C.S. Velden, N. Bormann, J.-N. Thepaut, L.P. Riishojgaard, Y. Zhu, and W.P. Menzel, 2003: Cloud-drift and water vapor winds in the polar regions from MODIS. IEEE Transactions on Geoscience and Remote Sensing, 41(2), 482-492.

Assimilation of Radial Wind measured by Doppler radar to Typhoon HIGOS

Masaru Kunii, Hiromu Seko

Meteorological Research Institute, Tukuba, Japan

1. Introduction

It is important to produce the accurate initial fields to improve the forecast of typhoons. Because the number of observation data near the typhoon center is not always large, the typhoon bogus data, which was produced empirically, has been used in producing initial fields. The typhoon bogus data improves the forecast effectively so that it is adopted in the 4-dimensional variational data assimilation (4DVAR) system for meso-scale model (MSM) of the Japan Meteorological Agency (JMA). However, there is some arbitrariness in setting the bogus parameters and thus the bogus data don't always express the actual state of the atmosphere. When the parameters are set improperly, the initial fields assimilated by actual observational data are contaminated by the typhoon bogus data. Conversely, when the large number of observed wind data is available the forecast of the typhoons is expected to be improved by assimilating the actual wind data into the models.

In this study, the radial wind (RW) data of Doppler radar, which are deployed by JMA for safety service of Airlines, are used as assimilation data. The impact of the RW data was investigated by comparison of typhoon tracks predicted from each analysis field.

2. Experiment design

In October 2002, the typhoon HIGOS passed by Narita and Haneda Doppler radars and thus the large number of radial wind data around the center of the typhoon was obtained. The observed RW data was assimilated into MSM by 4DVAR system of JMA. In this study, the assimilation method followed that of Seko *et al.* (2004). Namely, "super observation method" was adopted because the number of RW data was much larger than that of the model grids.

3. Impact of RW data

Figure 1 shows the RW at the elevation angle of 1.1 degree. The boundary between the negative and positive radial winds, namely zero velocity line, in the assimilated fields was similar to the observed ones. This similarity indicates that the RW data was assimilated appropriately. Figure 2 shows the typhoon tracks predicted from each analyzed fields. The track predicted from the RW-assimilated field was close to that of the typhoon bogus case. This result indicates that actual observed RW data can improve the forecast as much as the

typhoon bogus data.

However, there are two problems to be solved. One is the observational error of the RW data. The observation error was estimated by comparison of the observed RW and the predicted RW in a few case studies. More data assimilation experiments should be performed to get statistically appropriate observational errors. The other is the height fluctuation of RW data in an assimilation window. The locations of the observed RW data are geometrically determined. On the other hand, the MSM adopts σ -p coordinates system. Thus, the conversion is needed between these data. In this study, height is assumed to be constant for a period of an assimilation window (3-hour), and the position of RW data was converted with the first guess value. This assumption is acceptable when the change of height is much smaller than the width of radar beam. In this case study, the typhoon passed near the radar sites. Therefore the change of height should have been taken into account.

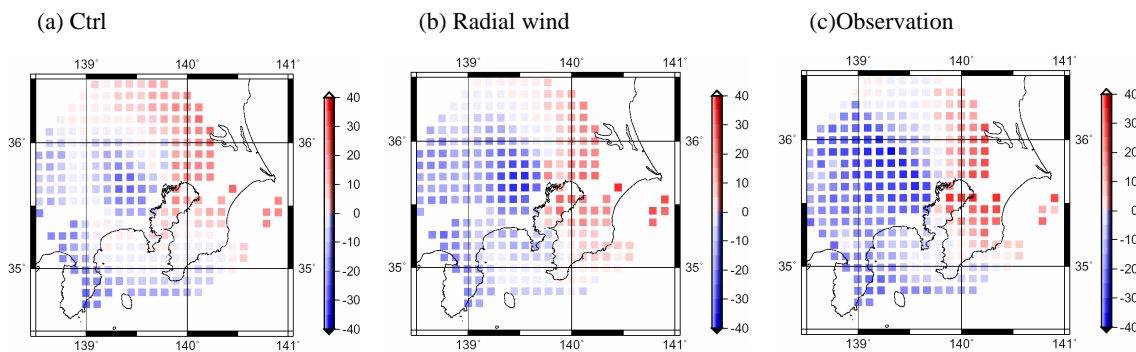


Fig. 1 Radial wind of the elevation angle of 1.1 degree. (a)Control run case in which the RW data and typhoon bogus data was not assimilated. (b)Radial wind case in which RW was assimilated. (c)Observed RW.

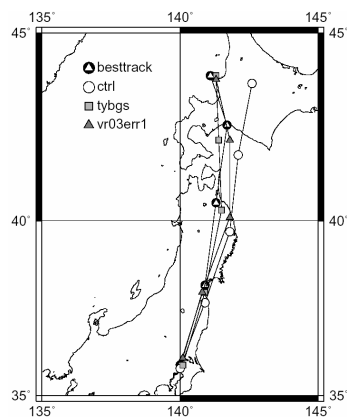


Fig. 2 Typhoon tracks predicted from each initial field and the best-track. "ctrl" is control run case in which the RW data and typhoon bogus was not assimilated. In the cases of "tybgs" and "vr03err1", the typhoon bogus and RW data were used, respectively. RW data were assimilated under the assumption that the variation of the height field for 3 hours (assimilation window length) had been trivial. The observational error of the RW data was tentatively set to actual Doppler radar error.

References

[1]Seko et al. 2004 : Impacts GPS-derived Water Vapor and Radial Wind Measured by Doppler Radar on Numerical Prediction of Precipitation. *J. Meteor. Soc. Japan* **82** ,473-489.

[2]JAPAN METEOROLOGICAL AGENCY 2002: OUTLINE OF THE OPERATIONAL NUMERICAL WEATHER PREDICTION AT THE JAPAN METEOROLOGICAL AGENCY. p15.

Corresponding author address : Masaru KUNII, Meteorological Research Institute, 1-1 Namigane Tukuba Ibaraki 305-0052, Japan email : mkunii@mri-jma.go.jp

Operational Implementation of 4D-Var at the Meteorological Service of Canada

Stéphane Laroche, Pierre Gauthier, Monique Tanguay, Simon Pellerin, Josée Morneau

Meteorological Service of Canada
Dorval, QC, CANADA

The three-dimensional variational data assimilation (3D-Var) for the operational medium-range forecasting system (Gauthier et al., 1999a; Chouinard et al., 2001) has been extended to 4D-Var. Presently, the Global Environmental Multi-scales (GEM) model is used in this forecasting mode with a uniform horizontal resolution of 0.9° and 28 vertical levels with a top at 10 hPa (Côté et al., 1998). The 4D-Var upgrade has been achieved by including the model integration as part of the observation operator, along with additional and improved features. First guess at the appropriate time (FGAT) from the full-resolution model trajectory is used to calculate the misfit to the observations. The tangent-linear of the GEM model and its adjoint (Tanguay and Polavarapu, 1999) are employed to propagate the analysis increment and the gradient of the cost function over the 6-h assimilation window. The analysis is obtained after two outer loops: 40 iterations with only the vertical diffusion as simplified linearized physics (Laroche et al., 2002) are first performed, then after updating the full-resolution trajectory, 30 more iterations are done with a set of simplified physical parameterizations which includes vertical diffusion, subgrid-scale orographic effects, large-scale precipitation and deep moist convection (Zadra et al., 2004; Mahfouf 2005). The data selection process has been modified for all observation types except the surface reports. The 6-h assimilation window is divided into 9 time intervals (rather than one in 3D-Var). For each interval, the data are spatially thinned to retain the observation closest to the middle of the time interval. This has considerably increased the number of frequently reported data such as aircraft, satwind and profiler data. Finally, the resolution of the analysis increment (T108), background error statistics (Gauthier et al., 1999b) and the data quality control remain the same as in 3D-Var (Gauthier et al., 2003).

An extensive pre-implementation evaluation of 4D-Var against the operational 3D-Var was conducted. Anomaly correlation scores for two-month assimilation periods in winter 2003-2004 and summer 2004 are presented in Fig. 1. A consistent improvement in the northern hemisphere and nearly 9-h gain in predictability in the southern hemisphere have been obtained with 4D-Var. The impact of 4D-Var is however rather neutral in the tropics (not shown). We found that about half of the improvement is explained by the use of the tangent-linear and its adjoint to properly propagate the information over the assimilation window. The other features of 4D-Var, that are the increased number of observations assimilated at the appropriate time, the use of a set of simplified physical parameterizations in the second outer loop and the trajectory update then explain (ranked in order of importance) the remainder of the overall improvement over 3D-Var. The 4D-Var will be implemented in the operational suite of the Canadian Meteorological Center by mid March 2005.

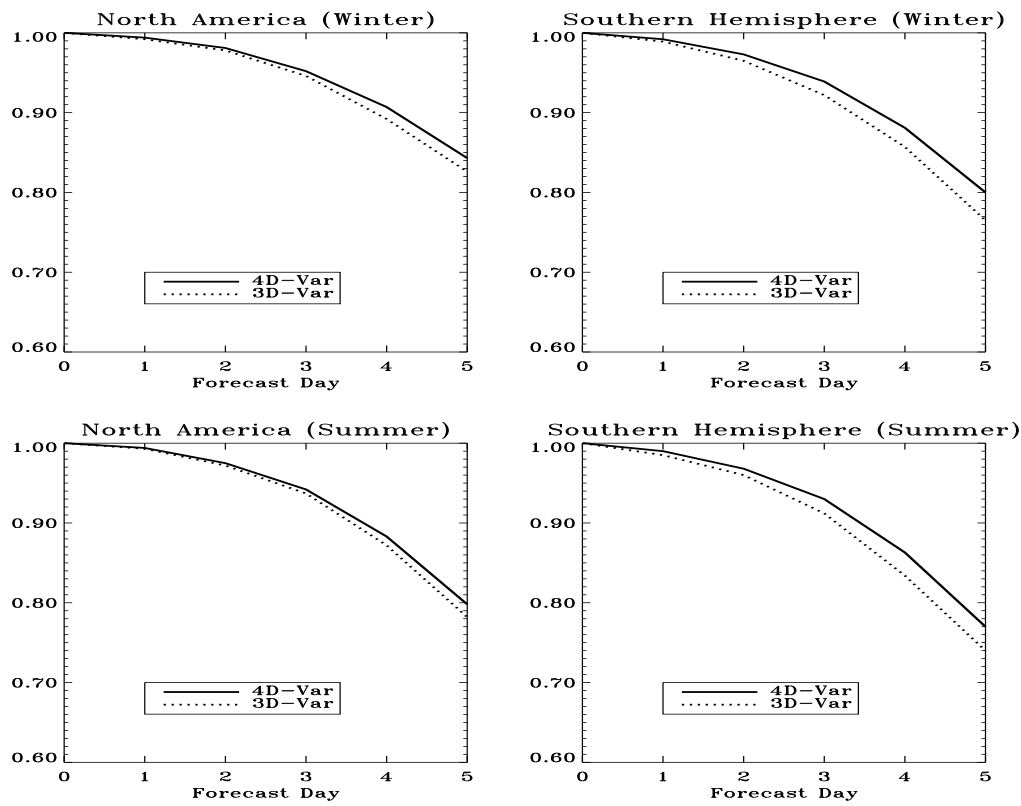


Figure 1. Anomaly correlation scores for 4D-Var and 3D-Var for the summer (15 Jul.-15 Sep. 2004) and winter (11 Dec. 2003-11 Feb. 2004) periods over North America and the Southern Hemisphere.

References

- Côté, J., S. Gravel, A. Méthot, A. Patoine, M. Roch and A. Staniforth, 1998: The operational CMC/MRB global environmental multiscale (GEM) model: Part I - Design considerations and Formulation. *Mon. Wea. Rev.*, **126**, 1373-1395.
- Gauthier, P., C. Charette, L. Fillion, P. Koclas, and S. Laroche, 1999a. Implementation of a 3D variational data assimilation system at the Canadian Meteorological Centre. Part I : the global analysis. *Atmosphere -Ocean*, **37**, 103-156.
- Gauthier, P., M. Buehner and L. Fillion, 1999b: Background-error statistics modeling in a 3D variational data assimilation scheme: Estimation and impact on the analysis. In proceedings, ECMWF Workshop on diagnosis of data assimilation systems. ECMWF, pp. 131-145.
- Gauthier, P., C. Chouinard and B. Brasnett, 2003: Quality Control: Methodology and Application. *Data Assimilation for the Earth System*. R. Swinbank et al., Kluwer Academic Publishers. 177-187.
- Laroche, S., M. Tanguay and Y. Delage, 2002: On the linearization of a simplified planetary boundary layer parameterization. *Mon. Wea. Rev.*, **127**, 551-564.
- Mahfouf, J-F., 2005: Linearization of a simple moist convection scheme for large-scale NWP models. To appear in *Mon. Wea. Rev.*
- Tanguay, M. and S. Polavarapu, 1999: The adjoint of the semi-Lagrangian treatment of the passive tracer equation. *Mon. Wea. Rev.*, **127**, 551-564.
- Zadra, A, M. Buehner, S. Laroche and J-F. Mahfouf, 2004: Impact of the GEM model simplified physics on the extratropical singular vectors. *Q. J. R. Meteorol. Soc.*, **130**, 2541-2569

Initialization with Rainfall defined Diabatic Heating

LEIMING MA*

Shanghai Typhoon Institute, China Meteorological Administration, Shanghai, China

*Email: malm@mail.typhoon.gov.cn

NOEL DAVIDSON

Bureau of Meteorology Research Center, VIC, Australia

YIHONG DUAN

JOHNNY CHAN

Shanghai Typhoon Institute, China Meteorological Administration, Shanghai, China

1. Introduction

Many studies have indicated that the inclusion of rainfall data into numerical models can improve the accuracy of numerical weather prediction (e.g. Zou 1996, Pu 2002). In this paper, the assimilation of NRL (US Naval Research Laboratory) rainfall is implemented with the idea of adjustment of diabatic heating to improve the large-scale environment and mesoscale structures in initial conditions. Numerical experiments are performed to evaluate the impact of rainfall data on the prediction of rainfall and track of Tropical Cyclone Chris, which made landfall near Port Headland, Western Australia during 3-6th, Feb. 2002.

The NRL rainfall data, classified as three types (i.e. stratiform, convective and composite rainfall - combined by stratiform and convective rainfall) following Churchill and Houze (1984), is used to define the vertical profiles of diabatic heating (Johnson 1984). The rainfall region is considered as convective type if the rainfall rate exceeds 10 mm h^{-1} . Grid points with a surface rainfall rate twice as large as the averaged value taken over the four surrounding grid points are identified as the convective type. During the period of initialization (assimilation), the diabatic heating from the cumulus scheme is replaced by the heating profile given by Johnson (1984) and 6-h satellite-observed cloud-top temperatures.

2. Experiment design

The BMRC (Bureau of Meteorology Research Center, Australia) tropical limited-area model (Davidson 1992) is used for the experiments. It is a hydrostatic, primitive equation model, with a vertical sigma coordinate system and semi-implicit time differencing. Physical parameterizations include a stability-dependent boundary layer, diurnally varying radiation with diagnosed surface temperatures over land, shallow convection, large-scale precipitation and Kuo-type cumulus convection. The horizontal grid spacing of 15 km and 29 sigma levels has been used in this study. Boundary conditions are obtained from the BMRC global prediction system.

Several experiments were performed with respect to the options of “rainfall assimilation” and “dynamic nudging” (Table.1). For the experiments RA (with rainfall assimilation) and RAN (with rainfall assimilation and dynamic nudging), 6-h accumulated NRL rainfall data are ingested in the model within each of the 4*6h initial (assimilation) periods, valid respectively at 24h, 18h, 12h, 6h prior to the base time of the simulation (23UTC 3 Feb 2002) (Fig. 1). To help make the momentum field more consistent with the mass field during the initialization, dynamic nudging (using conventional observations) is also performed in RAN.

3. Results

a. Rainfall distribution

Rainfall assimilation greatly improves the prediction of rainfall, with the RAN experiment the most obvious (Fig.2).

b. TC Track

Inclusion of NRL rainfall data improves the track in all the experiments (Fig. 3), with the RAN experiment

giving the most significant improvement.

References

- Churchill, D. D., and R. A. Houze, Jr., 1984: Development and structure of winter monsoon cloud clusters on 10 December 1978. *J. Atmos. Sci.*, 41, 933-960.
- Davidson, N. E., and K. Puri, 1992: Tropical prediction using dynamical nudging, satellite-defined convective heat sources, and a cyclone bogus. *Mon. Wea. Rev.*, 120, 2501-2522.
- Johnson, R. H., 1984: Partitioning tropical heat and moisture budgets into cumulus and mesoscale components: Implication for cumulus parameterization. *Mon. Wea. Rev.*, 112, 1590-1601.
- Pu, Zhaoxia, Tao, Wei-Kuo, Braun, Scott, Simpson, Joanne, Jia, Yiqin, Halverson, Jeffrey, Olson, William, Hou, Arthur. 2002: The Impact of TRMM Data on Mesoscale Numerical Simulation of Supertyphoon Paka. *Mon. Wea. Rev.*, 130, 2448-2458.
- Zou, X., Kuo, Y.-H.. 1996: Rainfall Assimilation through an Optimal Control of Initial and Boundary Conditions in a Limited-Area Mesoscale Model. *Mon. Wea. Rev.*, 124, 2859-2882.

Table.1 Design of numerical experiments

Numerical expt.	Rainfall assimilation?	Dynamic nudging?
CTRL	No	No
RA	Yes	No
RAN	Yes	Yes

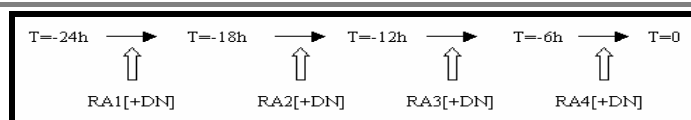


Fig.1 The cycle of rainfall assimilation

(RA1, RA2, RA3, RA4 denotes the assimilation with 6-h accumulated rainfall within each of the 4*6-h initialization periods, DN refers to the optional dynamic nudging)

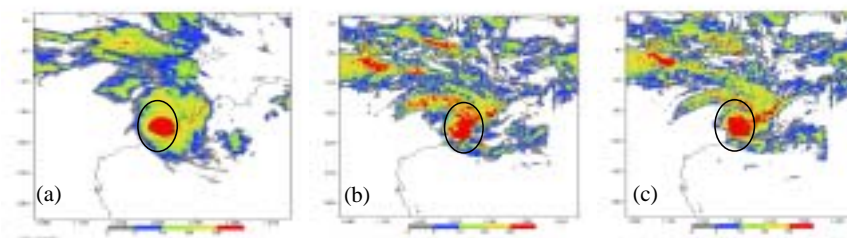


Fig. 2 (a) NRL accumulated rainfall and simulated rainfall in experiment (b) CTRL and (c) RA at 00UTC 3th – 00UTC 4th, Feb 2002. (the circle denotes the region of intensive rainfall)

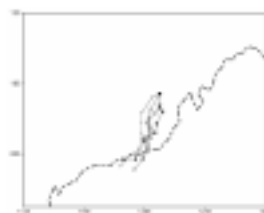


Fig.3 Observed and predicted tracks of Chris from 00UTC 3 Feb. 2002 at 6-h interval
The track with mark “open circle” denote the observation, “cross” - CTRL experiment,
“open square” - RAN experiment, “closed circle” - RA experiment.

Real data simulation of a thunderstorm over Kolkata using RAMS
P. Mukhopadhyay
Forecasting Research Division, Indian Institute of Tropical Meteorology,
Dr. Homi Bhabha Road, Pune-411008, INDIA

1. Introduction

Thunderstorm is one of the most frequent severe weather systems that affect eastern and north-eastern states of India. Due to smaller spatial and temporal dimension, thunderstorms are generally not resolved by conventional synoptic observational network of India. Consequently the prevailing instability that triggers the development of the system is often absent in the initial analyses. Model initialized with such initial condition fails to simulate/predict the system. Keeping this in view, an attempt is made to study the impact upper air and surface data on the simulation of 14 July 1998 thunderstorm over Kolkata using RAMS. The upper air stations namely Kolkata, Ranchi and Patna are located in the Gangetic plains in a suitable distance (~250-300 km) and there are number of stations over the region which provides surface observations. Two experiments are carried out to simulate the storm. In one of the experiment GAME analyses (0.5 x 0.5 lat-lon) is used to initialize the model and in the other upper air and surface data are blended to enhance the initial condition and subsequently the model is initialized with enhanced input.

2. Methodology

RAMS version 4.30 is used to carry out the simulation experiments. RAMS is used with two way interactive nested grids of resolutions 16 km and 4 km as shown in Fig. 2. The grids are centered at 22.6° N, 88.4° E and the number of grid points for 16 km resolution is 68 x 68 in east-west and north-south direction and that for 4 km grid are 58 x 58. The numbers of vertical terrain following levels in both the domains are 36. The height of the top of the model domain is 25 km. The vertical levels are stretched in the ratio 1.1:100; 2000 which implies the first level will have a thickness of 100 m, the next level will be of thickness 110 m and so on till the level reaches the thickness of 2000 m. The Klemp and Wilhelmson (1978) radiative boundary condition is applied in the lateral boundary and Davies (1983) nudging is applied as upper boundary condition. A Modified Kuo convection scheme (Tremback, 1990) is used for the large scale precipitation and Bulk microphysics of Walko et al. (1995) is used for prognosing cloud constituents and grid scale precipitation. A two-stream radiation scheme developed by Harrington (1997) is used. It allows interaction of three solar and five infrared bands with model gas constituents and cloud hydrometeors. The horizontal and vertical eddy diffusion coefficients are computed as the product of the 3D rate-of-strain tensor and a length scale squared. The length scale is the product of the vertical grid spacing and a constant. The model is initialized with 14 July 1998 0000 UTC analyses and run in FDDA nudging mode till 0600 UTC of 14 July and subsequently run in forecast mode till 1800 UTC of 14 July 1998.

3. Discussion of results

In the first experiment (EXP-1) the GAME analyses is interpolated to RAMS 16 km grid and model is run in nudging mode for initial 6 hour and in the other experiment (EXP-2), model is initialized with enhanced input and run in similar manner as in EXP-1. Simulation experiments suggest that the incorporation of the upper air and surface data have significantly improved the initial condition in terms better representation of the thermodynamic instability prevailing over the region. Different thermodynamic instability indices derived from the enhanced input is found to be closely matching with the values derived from the RSRW data of the stations (Kolkata, Ranchi and Patna). Mainly due to this improvement the 12 forecast by EXP-2 has significantly improved in comparison to that of EXP-1. Fig-3 shows the hourly evolution of x-z cross section of wind (u, w) and total cloud condensate (g kg^{-1}). It is seen from Fig. 3 that at 6, 7 and 8 hour forecast the vertical motion and total cloud condensate has reached a maxima. The total cloud condensate distribution even shows an anvil shape which is typical to such thunderstorm. More over the location of the storm at maturity is better simulated by EXP-2. Fig.4 shows 12 hour accumulated forecast precipitation. The precipitation distribution, amount and location is reasonably well simulated as compared to the observation The observed station rain gauge report at Kolkata is 5 cm.



Figure 1

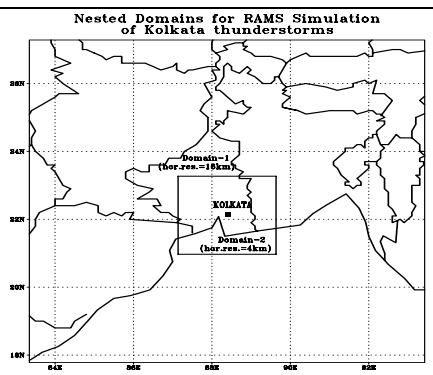


Figure 2

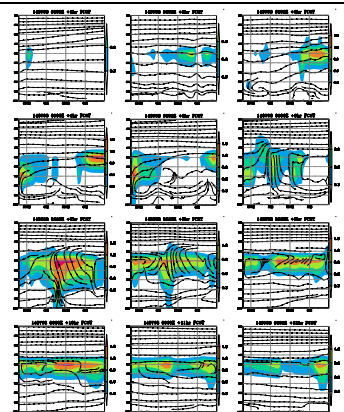


Figure 3

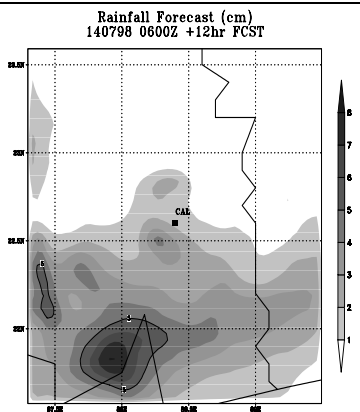


Figure 4

References

Klemp, J. B., and R. B. Wilhelmson, 1978a: "The simulation of three-dimensional convective storm dynamics". *J. Atmos. Sci.*, **35**, 1070-1096.

Davies, H. C., 1983: "Limitations of some common lateral boundary schemes used in regional NWP models". *Mon. Wea. Rev.*, **111**, 1002-1012.

Tremback, C. J., 1990: "Numerical simulation of a mesoscale convective complex: Model development and numerical results". PhD dissertation, Atmos. Sci. Paper No 465, Colorado State University, Department of Atmospheric Science, Fort Collins, CO 80523.

Harrington, J. Y. 1997: "The effects of radiative and micro-physical processes on simulated warm and transition season Arctic stratus". PhD Dissertation, Atmospheric Science Paper No 637, Colorado State University, Department of Atmospheric Science, Fort Collins, CO 80523, 289 pp.

Walko, R. L., W. R., Cotton, M. P., Meyers, and J. Y., Harrington, 1995: "New RAMS cloud microphysics parameterization Part I: the single-moment scheme". *Atmos. Res.*, **38**, 29-62.

Use of temperature data from radio-sonde observations in place of geopotential height in the JMA global 3D-VAR

A.Narui

Numerical Prediction Division, Japan Meteorological Agency

1-3-4 Otemachi, Chiyoda-ku, Tokyo 100-8122, JAPAN

narui@met.kishou.go.jp

1. Introduction

JMA has a plan to introduce the variational quality control of observational data (VarQC) (Andersson 1999) to the global analysis in the near future. Since it is favorable for the VarQC that there is no correlation among observational data, assimilation of temperature data from radio-sondes was tested in place of geopotential height, which has strong vertical correlation of observation errors. Though the main purpose of the work is to prepare for the introduction of VarQC, the use of temperature data showed positive impacts on forecast skill. The assimilation of temperature data from radio-sondes has been operational since 15th April 2004.

2. Modification to the assimilation system

Several modifications were made to the assimilation system to introduce the temperature data assimilation.

First we removed the vertical correlation of observation errors in radio-sonde data. Geopotential height data at a certain level are usually made from temperature data below that level so their errors are strongly correlated. On the other hand the other elements including temperature are observed independently so their errors are less correlated than geopotential height data. Therefore we can assume that all radio-sonde data are mutually non-correlated when using temperature data instead of geopotential height data.

Second we decided to use the data at significant levels in addition to the data at standard pressure levels. Because geopotential height data at a certain level are usually made from temperature data below that level, we should use as much temperature data as possible to conserve the information content.

Third we recalculated all the observation errors at each level from the statistics of the departure values between the observational data and the first guess i.e. 6hour forecasts (Dee and da Silva 1999). The period of the statistics is one year in 2002.

3. Parallel experiment

Parallel experiment to compare the performance of assimilation of radio-sonde temperature described above (Test) and that of radio-sonde geopotential height (Control) were conducted for one-month periods, July 2002 and December 2002, respectively. The model is global spectral model with the resolution of T213. The 216-hour forecasts were

conducted from 12UTC for each day from 1st July to 21st July and from 1st December to 21st December and anomaly correlation was calculated from these 21 forecasts for each period.

Figure 1 is the comparison of the anomaly correlation of 500hPa height between Test (red line) and Control (blue line) for July 2002. The anomaly correlation of Test is slightly better than that of Control in all the regions. Similar results were also obtained for December 2002.

4. References

Andersson, E., and H. Jarvien, 1999: Variational quality control, Q. J. R. Meteorol. Soc., 125, 697-722.

Dee, D. P. and A. M. da Silva, 1999: Maximum-likelihood estimation of forecast and observation error covariance parameters. Part I: Methodology. Mon. Wea. Rev., 127, 1822-1834.

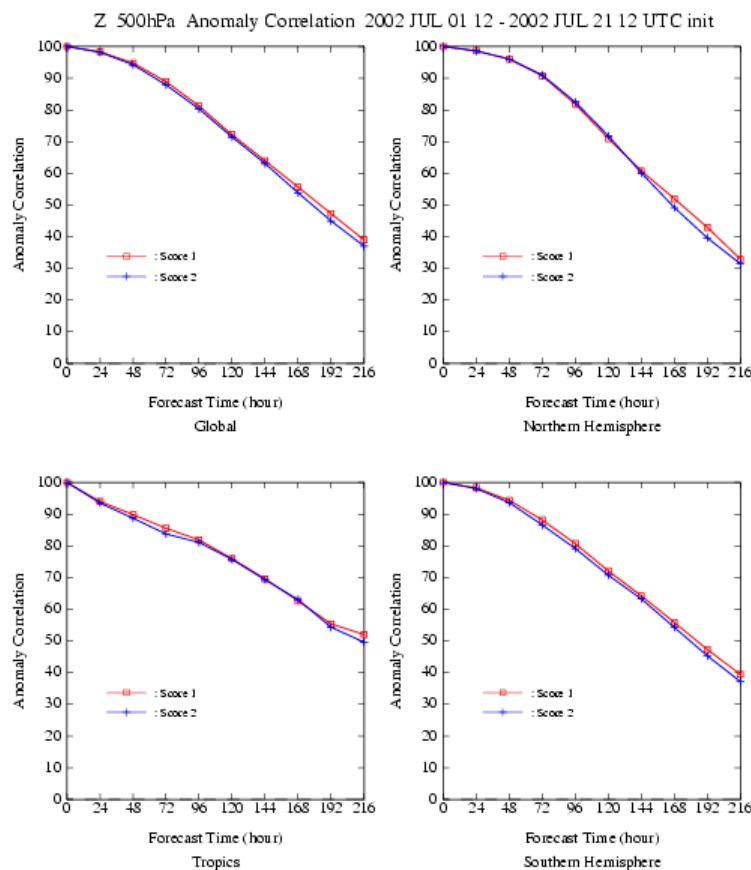


Fig.1 The comparison of the anomaly correlation(%) of 500hPa height of July 2002. The upper left panel is for the globe, the upper right one is for the northern hemisphere, the lower left one is for the tropics and the lower right one is for the southern hemisphere. The red line is for temperature assimilation (Test) and the blue line is for geopotential height assimilation (Control).

Operational Use of QuikSCAT / SeaWinds Ocean Surface Wind Data
in the Meso 4D-Var System

Yasuaki Ohhashi and Takao Imaizumi

Numerical Prediction Division, Japan Meteorological Agency

1-3-4 Otemachi, Chiyoda-ku, Tokyo 100-8122, JAPAN

e-mail: ohashi@naps.kishou.go.jp

A satellite-borne scatterometer obtains the surface wind vectors over the ocean by measuring the radar signal returned from the sea surface.

The QuikSCAT/SeaWinds ocean surface wind data have been used in operation since 6 May 2003 in the JMA global data assimilation system.

JMA has been operating a Meso-Scale Model with a 4D-Var data assimilation system. Data assimilation experiments of the SeaWinds ocean surface wind data were conducted using the Meso 4D-Var system. The assimilation experiments using the SeaWinds data were performed for each about two weeks started from 3 June 2003 and 1 February 2004. A quality control system for the SeaWinds data was the same as that in the global 3D-Var system. The data were thinned out to one datum at about 50 km intervals and used in the Meso 4D-Var system. Experiments with and without SeaWinds data are referred to as Test run and Control run, respectively.

Figure 1 shows the threat scores of rainfall forecasts over Japan. The threat scores both in June 2003 and February 2004 showed positive impact in the Test run in many forecast hours especially for heavy rain in summer.

Figure 2 shows an example of the SeaWinds observation and first guess wind field. The wind directions of the first guess were almost south-southwest. On the other hand, SeaWinds observed a shear line apparently over the East China Sea. The surface wind fields were analyzed more correctly by using the SeaWinds data (not shown in the figure). Figure 3 shows the 9 hour forecast field from the initial time 12 UTC 18 July 2003. The SeaWinds data shown in Figure 2 were used in the initial field of the Test run. It is evident that a heavy rain band along the shear line was well predicted in the Test run and showed better correspondence with the Radar-AMeDAS observation than that in the Control run.

Based on the above findings, QuikSCAT/SeaWinds data have been used in operation since 27 July 2004 at JMA.

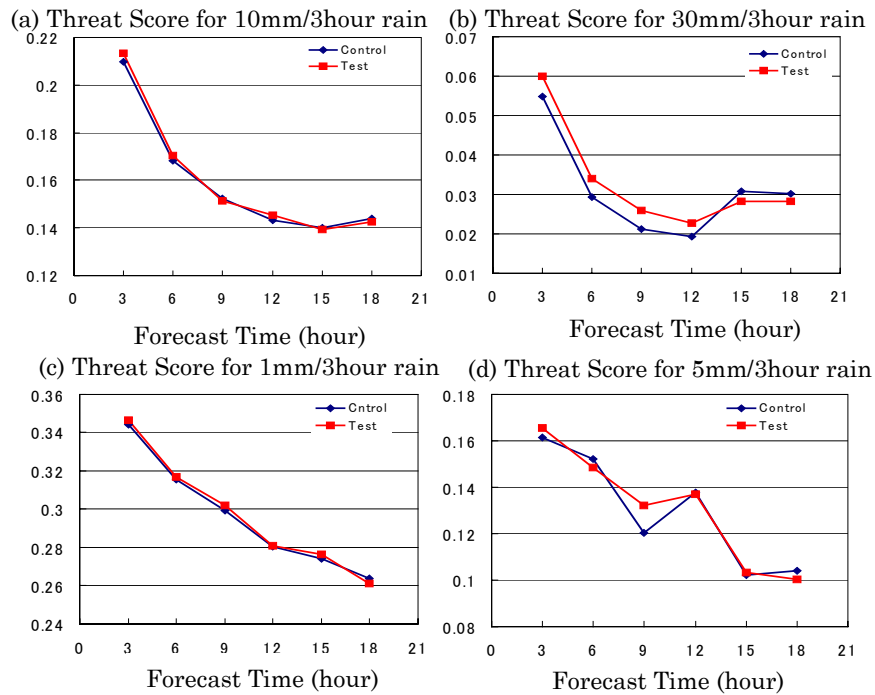


Figure 1. Threat scores for (a) moderate (10mm/3hour) and (b) heavy (30mm/3hour) rain for June 2003, Threat scores for (c) weak (1mm/3hour) and (d) moderate (5mm/3hour) rain for February 2004. Blue line denotes Control run and red line denotes Test run.

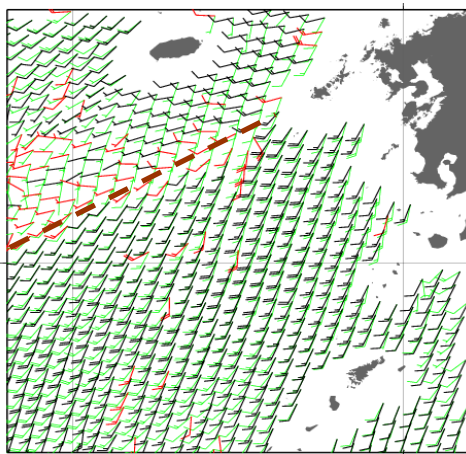


Figure 2. Black bars denote SeaWinds data and green bars denote first guess wind. Observation time is about 10 UTC 18 July 2003. Red bars are the data rejected in quality control. Full bars and half bars mean 5 and 10 knots, respectively. A brown dashed line denotes a shear line.

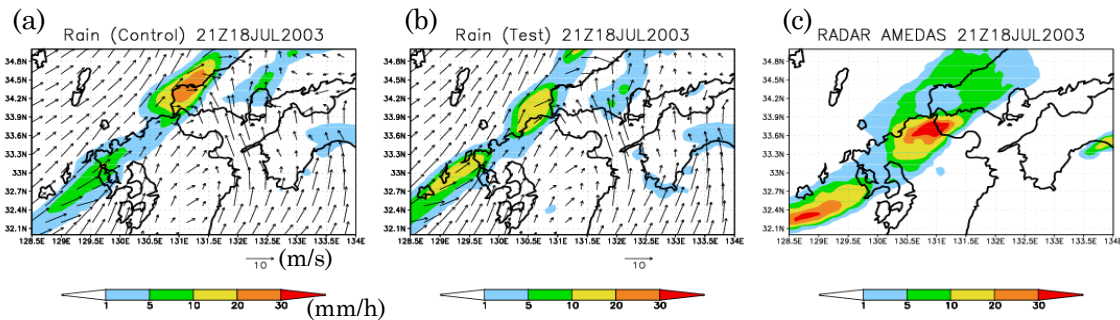


Figure 3. Horizontal distribution of hourly rainfall forecast and surface wind field after 9 hours from the initial time 12 UTC 18 July 2003. (a) Control run, (b) Test run, (c) Radar-AMeDAS rainfall observation at 21 UTC 18 July 2003.

A Global PSAS

A. Rhodin¹, D. Pingel¹, O. Schmid¹, M. Tomassini¹, H. Anlauf¹, W. Wergen¹,
M. E. Gorbunov², M. D. Tsyroulnikov³, L. Kornblueh⁴

¹ Deutscher Wetterdienst, Offenbach, Germany

² Obukhov Institute for Atmospheric Physics, Moscow, Russia

³ Hydrometeorological Research Centre of Russia, Moscow, Russia

⁴ Max-Planck-Institut für Meteorologie, Hamburg, Germany

A global PSAS (Physical Space Assimilation System) is under test at DWD and is planned to replace the OI (Optimum Interpolation) data assimilation currently operational for the Global Model (GME) at the German Weather Service.

PSAS

The PSAS is a 3-dimensional data assimilation system which minimizes the cost function as function of the control variables defined in observation space [2] [3]. Background- and observation-error covariances are represented in observation space as well. An advantage of this approach is the considerably reduced problem size (10^5 to 10^6 observations actually used compared to 10^8 degrees of freedom in model space). This allows a more flexible representation of the error covariance matrices and good pre-conditioning strategies (both background and observational error covariance matrices are accessible). The disadvantage is that the implementations of model equations, operators, and parameterizations in the forecast model cannot easily be used for observation operators and covariance modeling. Also an extension to a 4-dimensional variational assimilation is not straightforward. However, the extension to an Ensemble Kalman Filter assimilation system is an alternative.

Implementation

The assimilation system is implemented for the global model GME based on an icosahedral grid [6]. The PSAS algorithm does not depend on a particular grid and the adaption to other (regular) grids is straightforward; interpolation algorithms are implemented in a generic form. The program is coded in Fortran95 and parallelization is based on MPI (Message Passing Interface). At the German Weather Service the operational assimilation system runs on an IBM SP2.

The underlying set of linearized equations is solved by a CG (Conjugate Gradient) algorithm. In an outer loop a Newton algorithm accounts for the nonlinearities in the observation operators and in the Variational Quality Control (VQC), which is implemented following [1].

Background Error Covariances

Background and observation error covariance matrices are represented explicitly using a sparse representation. Currently background error correlations are modeled explicitly as a function of distance for geopotential height, relative humidity and wind components closely following the approach of the operational OI [4]. However this approach does not ensure positive definite matrices

because of the spatial variations of length scales of the correlation functions. (This has not been a problem in the OI because of its local formulation.) For this reason the explicit matrix representation will be replaced by an operator representation which ensures positive definiteness. Background correlations are initially estimated by the NMC method but will later be augmented by information from an ensemble system.

Observation Operators

Besides the conventional in situ observation operators (TEMP, SYNOP, AIREP, SATOB) the RTTOV [7] package is used for assimilation of satellite radiances. A 3-dimensional ray-tracing operator for the assimilation of bending angles from GPS radio occultations [5] is implemented as well.

References

- [1] E. Andersson and H. Jarvinen. Variational quality control. *Q. J. R. Meteorol. Soc.*, 125(554):697–722, 1999.
- [2] S. Cohn, A. Da Silva, J. Guo, M. Sienkiewicz, and D. Lamich. Assessing the effects of data selection with the DAO physical-space statistical analysis system. *Mon. Wea. Rev.*, 126:2913–2926, 1997.
- [3] R. Daley and E. Barker. Navdas source book 2000. Technical report, Naval Research Laboratory, Marine Meteorology Division, Monterey, CA 93943-5502, 2000.
- [4] ECMWF Research Department. *Research Manual 1 - ECMWF Data Assimilation Scientific Documentation*. ECMWF, 3rd edition, 1992.
- [5] M. E. Gorbunov and L. Kornblueh. Principles of variational assimilation of GNSS radio occultation data. Report 350, Max-Planck-Institut für Meteorologie, Bundesstrasse 55, D-20146 Hamburg, Dec. 2003.
- [6] D. Majewski, D. Liermann, P. Prohl, B. Ritter, M. Buchhold, T. Hanisch, G. Paul, W. Wergen, and J. Baumgardner. The operational global icosahedral-hexagonal gridpoint model GME: Description and high-resolution tests. *Mon. Wea. Rev.*, 130(2):319–338, Feb. 2002.
- [7] NWP-SAF. RTTOV radiative transfer model.
<http://www.metoffice.com/research/interproj/nwpsaf/rtm>.

Towards the use of Doppler radar radial winds in NWP

Kirsti Salonen
Finnish Meteorological Institute
kirsti.salonen@fmi.fi

1 Introduction

Present-day numerical weather prediction (NWP) models are global atmospheric models with resolutions from 20 to 50 km, and limited area models running with around 10 km resolutions. The interest and development in limited area NWP modelling focus increasingly on forecasting of quickly developing mesoscale phenomena in high resolution and observations are needed with high temporal and spatial resolution. Remote sensing observations are very appealing for this purpose because they have very good spatial and temporal coverage. This report concentrates on using Doppler radar radial winds in HIRLAM (High Resolution Limited Area Model) model.

2 Observation preprocessing

Doppler radars produce radial wind data with high temporal and spatial resolution. To correspond the observations to the often much coarser model resolution, some preprocessing is required. One method is to thin the raw observations to coarser resolution. The disadvantage of this method is that the resulting wind field can be very noisy, if the wind field is partly contaminated by non-meteorological echoes. Another possibility is to generate spatial averages, so called superobservations (SO), from the raw data. Superobservation generation averages out the random errors from the wind field quite effectively.

3 Observation operator

An observation operator for Doppler radar radial winds (Salonen et al., 2003) has been developed and implemented for the HIRLAM 3-dimensional variational assimilation system (Gustaffson et al., 2001). The formulation of the observation operator involves:

1. Horizontal and vertical interpolation of the NWP model wind components u and v to the observation location.
2. Projection of the interpolated NWP model horizontal wind towards the radar, and finally on the slanted direction of the radar beam.

The broadening of the radar beam is modelled by using Gaussian averaging kernel in the vertical interpolation. The obscuring effect of the radar horizon is taken into account by assuming a radar horizon of 0° elevation angle, below which the model information is not used. An empirical upper integration limit is set to 1.5 times the beamwidth. This is based on the fact that the radar reflectivity usually decreases rapidly above that height. Radar beam bending is taken into account by applying the Snell's law. The calculated effective elevation angle is used in the projection of the horizontal wind on the slanted direction of the radar beam. This approach modifies also the observation height from the value obtained by applying the $\frac{4}{3}r$ -law.

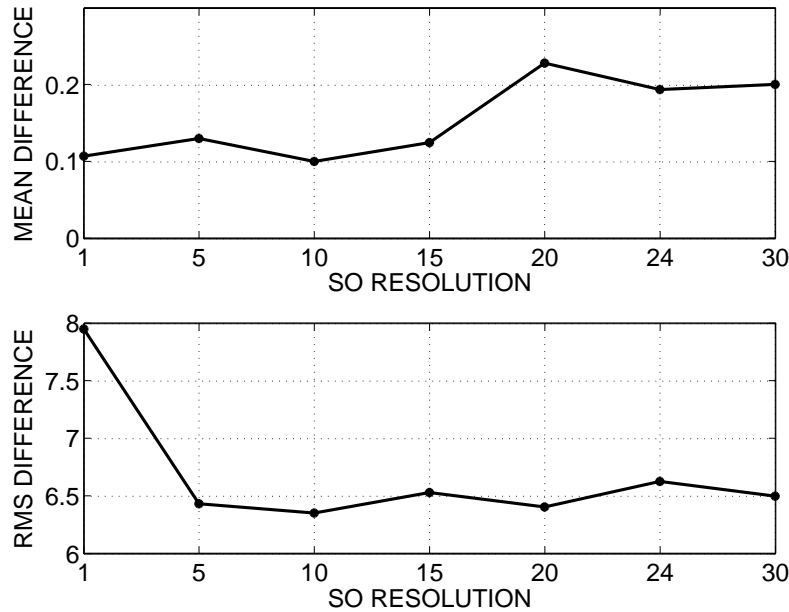


Figure 1: Mean (upper figure) and rms (lower figure) difference between the observations and the model counterpart as a function of SO resolution.

4 Optimal SO resolution

A set of one month (January 2002) experiments have been performed to study the fit of the SOs generated with different resolutions to the model counterpart calculated from HIRLAM model. SOs are generated with 5 km, 10 km, 15 km, 20 km, 24 km and 30 km resolutions, and also thinned raw data is studied. The model resolution is 22 km on 40 vertical levels.

Figure 1 shows the mean and the rms difference between the SOs and the model counterpart as a function of SO resolution. Resolution 1 km corresponds to the thinned raw data. In general, the mean difference is always positive, i.e. the observed wind is stronger than the modelled wind. The mean difference is smallest for the SO resolution of 10 km. The rms difference for the thinned raw data is approximately 1.5 m/s higher than the rms difference for any of the SO resolutions. One reason for this behaviour is that in the SO generation the random errors are averaged out quite effectively. Another possible source of rms difference is that the raw data includes wind field variations which are not represented in the 22 km resolution model.

References

- Gustafsson, N. and Coauthors, 2001: Three-dimensional variational data assimilation for a limited area model. Part I: General formulation and the background error constraint. *Tellus*, **53A**, 425-446.
- Salonen, K., H. Järvinen and M. Lindskog, 2003: Model for Doppler radar radial winds. *31st American Meteorological Society Conference on Radar Meteorology Volume I*, 142-145.

Data Assimilation Experiments of Nerima Heavy Rainfall

Hiromu Seko^{*a}, Takuya Kawabata^a, Tadashi Tsuyuki^b

^a Meteorological Research Institute, Japan Meteorological Agency, Tsukuba, Japan

^b Numerical Prediction Division, Japan Meteorological Agency, Tokyo, Japan

1. Introduction

Because the thunderstorms in the urban areas sometimes cause the heavy rainfall, the precise forecast of their generation and development is needed. It is well known that the low-level convergence of moist air generates and develops the thunderstorms. Thus, it is expected that assimilation of the low-level convergence and moist air improves the forecast of the thunderstorms. In this study, the radial wind (RW) observed by Doppler radar and precipitable water vapor (PWV) derived from ground-based GPS were used as the assimilation data. When these data were assimilated by 4-dimensional data assimilation system for Mesoscale Spectral Model (MSM-4dVarDAS) of Japan Meteorological Agency (JMA), the time, position and shape of the precipitation regions that included the heavy rainfall at Nerima/Tokyo was reproduced. However, the precipitation intensity was much weaker than the observed one.

To reproduce intensity of the heavy rainfall, the non-hydrostatic model of JMA (NHM) that predicts water substances explicitly was used, and the RW and PWV was assimilated into NHM by 3-dimensional data assimilation system (NHM-3dVarDAS).

2. 'Nerima heavy rainfall'

On 21 July 1999, the Baiu front over the northern part of the Japan moved southward slowly. When the precipitation of the Baiu front entered the Kanto region, the convective system that had a horizontal scale of several ten kilometers was generated at the southern Kanto area at 15JST (Fig. 1). This convective system developed and the heavy rainfall of 111.5 mm/hour was observed at Nerima/Tokyo at about 16JST. When the intense convections were developed, the easterly and northerly flows were observed in the precipitation regions. The southwesterly inflow from the south converged with them along the southern edge of the precipitation regions. These precipitation regions began to decay from 17JST and weak precipitation areas remained until 21JST.

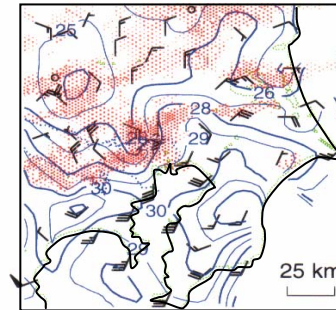


Fig. 1 Horizontal distribution of precipitation region (shade), surface temperature (solid line) and horizontal wind at 16JST 21 July

3. Impacts of RW and GPS-derived PWV

Because the heavy rainfall over the southern Kanto area was composed of well-developed convective cells, the horizontal grid interval of NHM was set to be 5km express the individual convective cells. Horizontal grid number was set to be 122 × 122 so that the simulation domain covered the whole Kanto area. Number of vertical layers was 45. The depth of the layer was stretched from 20 m to 1450 m from the surface to the upper boundary.

When the simulation was performed by NHM from the initial fields produced from the MSM-4dVarDAS-derived analyzed fields, however, the intense precipitation was not generated over the southern Kanto (not shown). Although the convergence of the horizontal wind was reproduced by MSM-4dVarDAS, the updraft estimated from spatial interpolated horizontal wind was too weak to saturate the water vapor. So as to reproduce intense updraft, RW observed by Doppler radars was assimilated into the initial fields of 15 JST by NHM-3dVar-DA system (Miyoshi, 2003). The production methods for assimilation data and observation operator are almost same as Seko et al., 2002, although observation errors of RW and PWV were reassessed.

The precipitation fields predicted from the results of NHM-3dVarDAS are shown in Fig. 2. The analyzed field at 15 JST shows that the southerly wind converged at the southern Kanto area. However, precipitation was not generated though the updraft was strengthened.

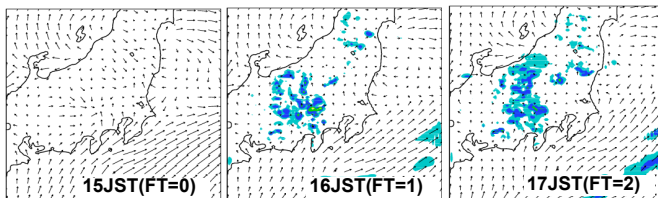


Fig. 2 Hourly precipitation and horizontal wind at 0.5 km from 15 JST to 17 JST on 21 July 1999 predicted by NHM.

4. Introduction of convective-cell-scale water vapor distribution and initial rain water and snow

In NHM-3DVarDAS, water vapor was not related to the updraft velocity to avoid the generation of unrealistic waves over the mountain areas. Therefore, water vapor in the intense updraft regions was not always saturated by NHM-

* hseko@mri-jma.go.jp, phone +81-29-853-8640; fax +81-29-853-8649

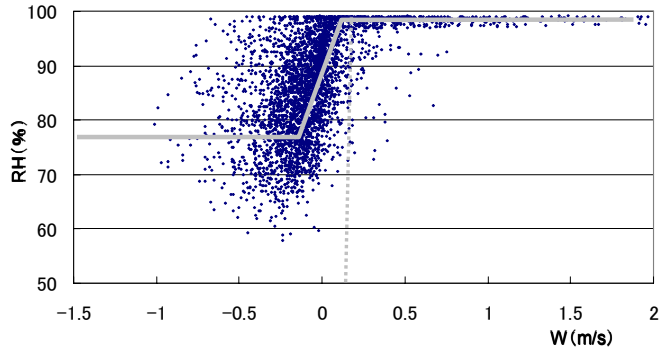


Fig.3 Scatter gram of simulated RH and updraft velocity within the precipitation region in the ranges of Doppler radar produced from the output of the NHM.

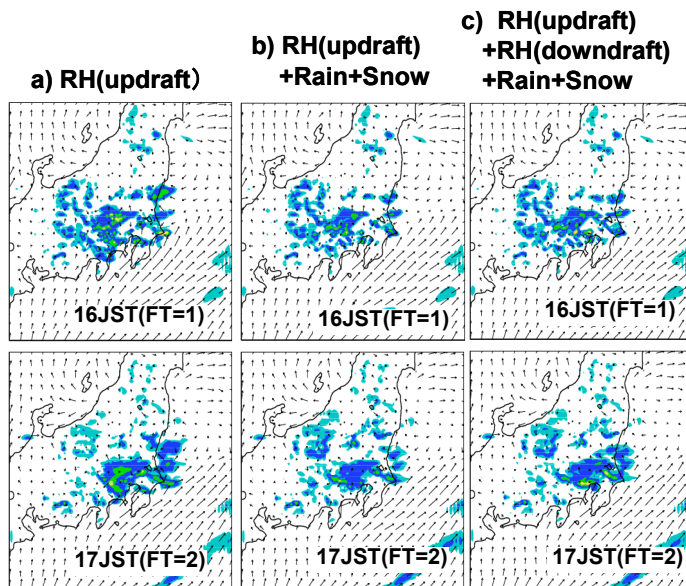


Fig. 4 Impact of introducing the convective cell scale water vapor distribution and initial water substances.

vapor and initial water substances. When the rain water and snow were introduced, the northwestern part of the precipitation region, which was decaying at 17 JST, was well reproduced. Furthermore, when the RH at the downdraft grids was changed, the convections along the southern edge of the precipitation region, which were produced by the outflow from the decaying region, were more developed. These simulated features were common to the observed ones. These similarities of precipitation intensity were maintained until 20 JST.

5. Summary

In these data assimilation experiments, the impacts of convective-cell-scale water vapor and the initial water substances on the precipitation prediction of a heavy rainfall were investigated. The comparison with the observed precipitation field indicates that convective-cell-scale water vapor and the introducing the rain water and snow should be considered in reproducing the convective cells of heavy rainfall.

References

- Miyoshi, T. "Development of JNoVA0 (three dimensional data assimilations system)", *Suuchiyohouka-houkoku, bettusatsu* **49**, pp148-155, 2003 (in Japanese)
- Ishikawa, Y., "Development of a mesoscale 4-dimensional variational data assimilation (4D-Var) system at JMA". *Proc. of the 81st Annual Meeting of AMS: Precipitation Extremes: Prediction, Impacts, and Responses*, P2.45, 2001.

3DVarDAS. In order that the relation between water vapor and updraft velocity is given to the analyzed fields, the scatter gram of simulated Relative humidity (RH) and updraft velocity within the precipitation regions within the radar ranges was obtained from the outputs of the NHM (Fig. 3). Because water vapor where the updraft exceeded 1.5 m/s was saturated, water vapor at updraft grids within the observed precipitation region was set to be saturated. This relation also means that intense updraft was maintained by convections. When the numerical simulations were performed from this modified initial condition, precipitation over the southern Kanto area was reproduced (Fig. 4a). However, the northwestern part of the precipitation region developed too intensely, while the observed northwestern part was decaying at 15 JST. This overdeveloped precipitation was due to the relation between the RH and updraft velocity that cannot express the evolution of convections.

So as to express the evolution of convective cells, rain water, snow and RH in the downdraft region were introduced. In general, there is large amount of rain water and snow, which weaken the updraft, in the well-developed convections. Thus, rain water and snow were estimated from the observed reflectivity fields, and then portioned according to the analyzed temperature. Namely, if the temperature was below 0 degree, snow was given at the grid points where the reflectivity was observed. It is known that the low-level cold outflow was produced by evaporation of water substances in dry downdraft regions. The low-level cold outflow helps develop the intense convections through the intensification of low-level convergence. Thus, the relation between the RH and downdraft was also obtained from the scatter gram, and then the RH in the downdraft region within the precipitation regions was changed according to the relation. Figures 4b and 4c show the impacts of introducing the convective-cell-scale water

Assimilation of Radar Data in the Mesoscale NWP-Model of DWD

Klaus Stephan, Stefan Klink, Christoph Schraff

Deutscher Wetterdienst, Kaiserleistr. 29/35, 63067 Offenbach am Main, Germany

e-mail: klaus.stephan@dwd.de, stefan.klink@dwd.de, christoph.schraff@dwd.de

The Lokal-Modell (LM) of DWD is a non-hydrostatic meso-scale model for short-range numerical weather prediction (NWP). Operationally, its initial state is generated by an assimilation scheme based on the nudging technique. Using non-gridded conventional observations, the focus is on the analysis of meso-alpha-scale structures.

In view of the development of a very high-resolution version of LM (so called LMK) dedicated to very short-range NWP of severe weather, high-resolution precipitation data derived from radar networks are introduced in the assimilation. The aim of this approach is to assimilate observed meso-gamma-scale structures and adjust the moist processes in order to improve the quantitative precipitation forecasting (QPF). Radar data, currently used for the assimilation, is a composite based on the precipitation scans of the 16 German radars (spatial mesh: $\sim 1 \text{ km} \times 1 \text{ km}$, time resolution 5 min).

Using the Latent Heat Nudging (LHN) technique, the thermodynamic quantities of the atmospheric model are adjusted in such a way that the modelled precipitation rates resemble the observed precipitation rates. This adjustment scheme works locally, because it is based on the assumption that in a vertical column, the integrated release of latent heat is proportional to the precipitation rate at the ground. Based on the quotient of observed over modelled precipitation rate a temperature increment is calculated in such a way that heating will take place at grid points where modelled precipitation is below the observed one. The LHN approach implemented in LMK is based on the algorithm described in Jones and Macpherson (1997). Their algorithm has been operationally and successfully used at the UK MetOffice since April 1996 (Macpherson, 2001).

Current schemes for gridscale precipitation often assume a column equilibrium for sedimenting constituents (Gassmann, 2002). That is, sedimentation can be considered to be a fast process compared to the characteristic time of cloud development. In the model's framework precipitation is falling to the bottom model level within one single time step. Below, this scheme will be referred to as "diagnostic". When increasing the model's spatial resolution, the assumption of column equilibrium for the precipitating constituents becomes more and more unrealistic. 3D advection and interactions between the different kinds of hydrometeors have to be considered within a "prognostic" precipitation scheme.

Figure 1 compares hourly precipitation amounts for the 9th of June 2004 8-9 UTC derived from radar measurement (b) with different assimilation runs. Figure 1a shows a control run without LHN, the lower panels show two runs with LHN. In fig. 1c a simulation with a diagnostic precipitation scheme is presented and in fig. 1d a simulation with prognostic precipitation. The results from this case study show that precipitation patterns are introduced in the analysis (data assimilation mode) in good agreement, both in position and amplitude, with those observed by radar if the model calculates the precipitation diagnostically. Particularly during the assimilation, the performance of LHN becomes worse if a prognostic treatment of precipitation is deployed. The major challenge seems to be the lagged model feedback on the LHN increment, which is caused by the fact, that precipitation, simulated by a prognostic scheme, needs some time to reach the ground. Therefore the LHN algorithm does not notice if precipitation has been increased or reduced so far, which mainly leads to a strong overestimation of precipitation.

The features of the prognostic precipitation scheme have a tremendous effect on the LHN algorithm. The algorithm assumes a strong correlation between the integral of the latent heat release within a vertical column and the precipitation rate at the bottom of the same column. Such a correlation is found for model runs with a diagnostic precipitation scheme and is shown in fig. 2a. Since we have used a prognostic precipitation scheme the basic assumption is no longer valid within one vertical column. Figure 2b gives the impression that the precipitation pattern is slightly shifted upstream of the pattern of vertical integrated latent heat rate. Thus one has to adopt the former LHN algorithm on the new specifications due to the prognostic precipitation scheme. Work is underway to find out how this can be achieved.

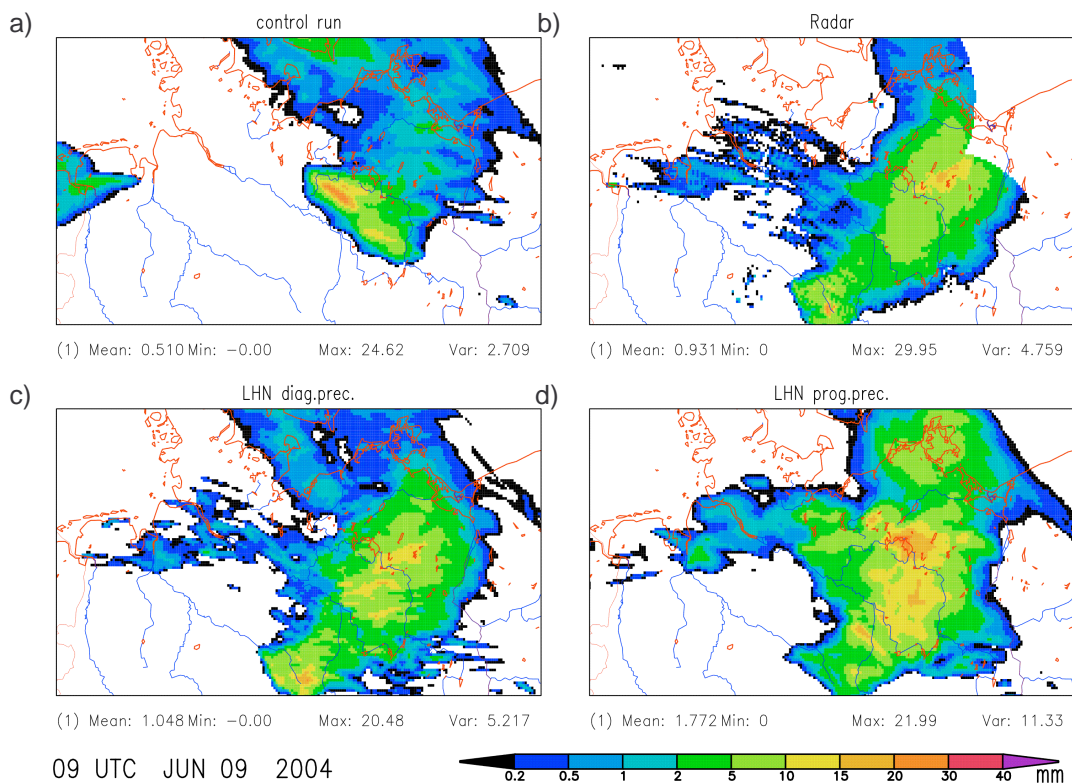


Figure 1: hourly precipitation sums for 9th June 2004 08-09 UTC, control run (assimilation mode) (a), Radar observation (b), LHN run with diagnostic precipitation (assimilation mode) (c) and LHN run with prognostic precipitation (assimilation mode) (d).

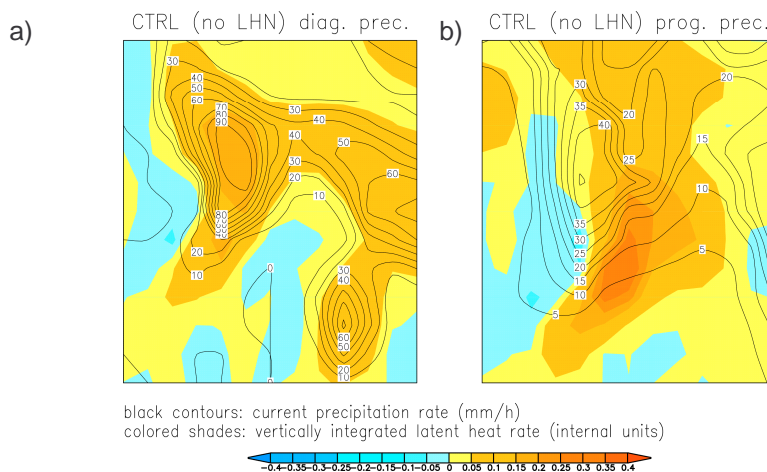


Figure 2: horizontal patterns of current precipitation rate and vertically integrated latent heat rate for a simulation with diagnostic precipitation (a) and with prognostic precipitation (b).

References

- Jones, C.D. and Macpherson, B., 1997: A Latent Heat Nudging Scheme for the Assimilation of Precipitation Data into an Operational Mesoscale Model. *Meteorol. Appl.* **4**, 269-277.
- Macpherson, B., 2001: Operational Experience with Assimilation of Rainfall Data in the MetOffice Mesoscale Model, *Meteorol. Atmos. Phys.*, **76**, 3-8.
- Gassmann, A., 2002: 3D-transport of precipitation. *COSMO Newsletter*, **2**, 113-117 (available at www.cosmo-model.org).

Assimilation of SEVIRI infrared observations at ECMWF

Matthew Szyndel¹, Jean-Noël Thépaut and Graeme Kelly

Infrared data observed from geostationary orbit is assimilated into the ECMWF integrated forecast system (IFS) with positive impact in the form of Meteosat clear sky radiance data and GOES Imager clear sky brightness temperature data (Köpken *et al.*, 2004). These data provide not only upper tropospheric humidity data, but also wind information through the use of a 4D-Var assimilation system (Courtier *et al.*, 1994) and the temporally dense nature of geostationary observations. In January 2004 Meteosat-8 became the first operational Meteosat second generation (MSG) satellite. MSG satellites carry the spinning enhanced visible and infrared imager (SEVIRI) (Schmetz *et al.*, 2000), an instrument with a range of visible and infrared channels including two channels sensitive to water vapour. We carried out assimilation experiments to assess the impact of assimilating Met-8 water vapour channel data in place of Met-7 data into the ECMWF IFS. Following these assimilation experiments Met-8 data from channels WV6.2 and WV7.3 were routinely assimilated into the IFS in place of Met-7 data from channel WV from 28th September 2004. Full details may be found in Szyndel *et al.*, 2004.

Our assimilation experiment was run for the period 2nd February 2004 to 2nd March 2004 and compared four streams of assimilation and forecast; these streams were:

1. 'Esuite' - operational test bed in use at the time of the experiment.
2. 'Control' - as esuite with Met-7 WV data blacklisted.
3. 'SEVIRI 1' - as 'Control' with Met-8 WV6.2 assimilated with 2K error and WV7.3 assimilated with 2K error.
4. 'SEVIRI 2' - as 'Control' with Met-8 WV6.2 assimilated with 2K error and WV7.3 assimilated with 1.5K error.

The assimilation of Met-8 data produced stronger increments than Met-7 data, with the increments over a wider area. This applies to increments in both relative humidity and vector winds. Relative humidity increments showed an increase in vertical structure, which is attributable to the use of two channels for each observation point where only one was used for Met-7. Relative humidity increments are shown in figure 1.

Over the period of the trial it was found that SEVIRI 1 and SEVIRI 2 both gave a small positive impact, with statistically significant impact on vector wind RMS error and geopotential height anomaly correlation at a number of pressure levels. Furthermore, studies of the impact on statistics for radiosonde observations show a reduction in bias of observation difference from model first guess for relative humidity observations in the area observed by Met-8. AMSU-B channel 3 observations and HIRS channel 12 observations show a reduced standard deviation of observation minus first guess in the Met-8 observed region. Figure 2 shows the impact of Met-8 assimilation on the standard deviation of (O-B) for HIRS-12 on NOAA-16.

Stream SEVIRI 1 was chosen for operational use as this stream showed marginally better impact.

¹ matthew.szyndel@ecmwf.int

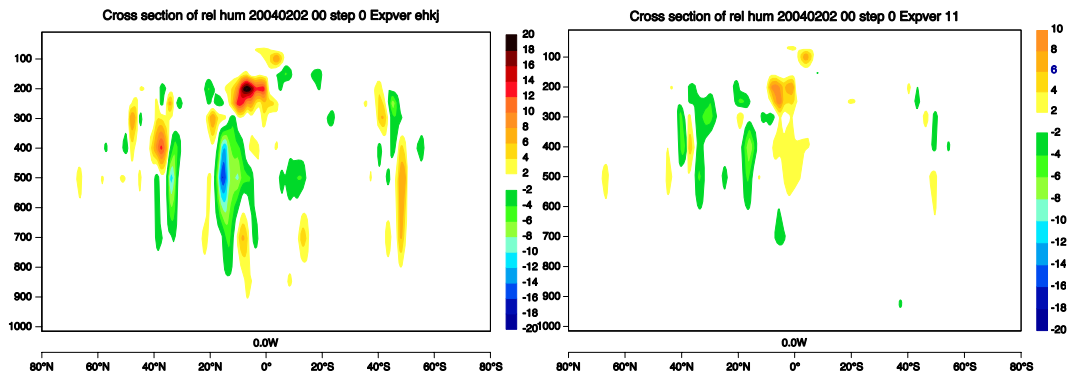


Figure 1: Relative humidity increment (in percent) for a cross section through the 0° meridian for the first cycle due to Met-8 in stream SEVIRI 1 (left panel) and Met-7 in stream esuite (right panel).

STATISTICS FOR RADIANCES FROM NOAA-16 / HIRS - 12
 STDV OF FIRST GUESS DEPARTURES (CLEAR)
 DATA PERIOD = 2004020118 - 2004022912 , HOUR = ALL
 EXP = EHL0
 Min: -3 Max: 2.4339

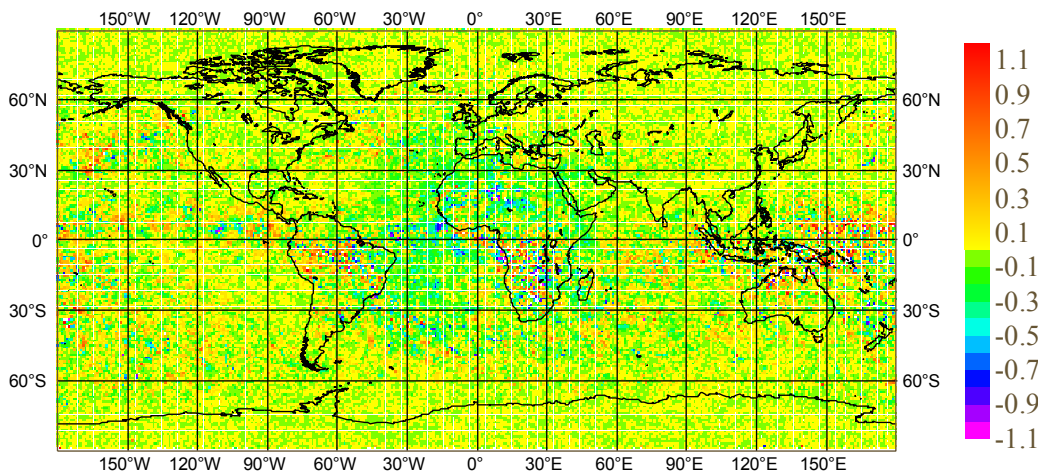


Figure 2: Change in standard deviation of (Observation - First Guess) for HIRS channel 12 on NOAA-16 as a result of Met-8 assimilation (stream SEVIRI 1)

Courtier, P., Thépaut, J.-N. and Hollingsworth, A., 1994: A strategy for operational implementation of 4D-Var, using an incremental approach, *Q. J. R. Meteorol. Soc.*, **120**, 1367-1387

Köpken, C., Kelly, G. and Thépaut, J.-N., 2004: Assimilation of Meteosat radiance data within the 4D-Var system at ECMWF: Assimilation experiments and forecast impact, *Q. J. R. Meteorol. Soc.*, **130**, 2277-2292

Schmetz, J., Pili, P. and Tjemkes, S., 2000: Meteosat Second Generation (MSG) Pp. 111-121 in proceedings of ECMWF seminar on exploitation of the new generation of satellite instruments for numerical weather prediction, 4-8 September 2000, ECMWF, Reading, UK

Szyndel, M.D.E., Kelly, G. and Thépaut, J.-N., 2004: Assimilation of Geostationary WV Radiances from GOES and Meteosat at ECMWF, EUMETSAT/ECMWF Fellowship Programme, Research Report No. 14

Use of AMSR-E Data in the JMA Operational Meso Analysis

Toshiharu Tauchi*, Yoshiaki Takeuchi, Yoshiaki Sato
Numerical Prediction Division, Japan Meteorological Agency
1-3-4 Otemachi, Chiyoda-ku, Tokyo 100-8122, JAPAN
e-mail:ttauchi@naps.kishou.go.jp

The Japan Meteorological Agency (JMA) has been operating a Meso-Scale Model (MSM) with the 4D-Var data assimilation system (Meso 4D-Var) since March 2002. This model is utilized for very short range rainfall forecasts to mitigate natural disasters.

A data assimilation method for rain rate (RR) and total column precipitable water (TCPW), which are retrieved from SSM/I and TMI, has been introduced since October 2003 (Sato et al. 2004). It brought the information of water vapor distribution over the ocean into MSM, and contributed to improvement of the rainfall forecast.

In addition to SSM/I and TMI, the AMSR-E data of Aqua satellite has become available with the cooperation between JMA and JAXA¹. The AMSR-E data consists of the RR and TCPW data like the SSM/I data with different observation times. Therefore, AMSR-E complements the data coverage, and it would contribute to further improvement of the forecast.

Some observation system experiments with the AMSR-E data were performed. To retrieve both RR and TCPW, the method developed by Takeuchi and Kurino (1997) was employed. It was the same as the method for SSM/I and TMI. Figures 1 and 2 show the case of heavy rain. It occurred on 17 July 2004. Figure 1a shows the analyzed water vapor field without the AMSR-E data at 18 UTC 17 July 2004 and Figure 1b shows the one with AMSR-E. With the AMSR-E assimilation, the water vapor was increased over the area A and decreased over the area B. Figure 2a shows the rainfall forecasts with the initial condition without AMSR-E, and Figure 2b shows the one with AMSR-E. Figure 2c shows the corresponding radar observation. Without the AMSR-E assimilation (Fig. 2a), the amount of the rainfall forecast in Fukui Area (indicated by arrows) was much smaller than that of the observation. By assimilating AMSR-E (Fig. 2b), more precipitation was predicted, and it was closer to the radar observation.

The threat scores of weak rain(1mm/3hour) over Japan area are shown in Fig. 3. The score showed positive impact on the almost all forecast times in both summer and winter experiments.

With the above results, JMA decided to use the AMSR-E data in the operation of MSM and it has started in November 2004.

References:

- Takeuchi, Y and T. Kurino, 1997: "Document of algorithm to derive rain rate and precipitation with SSM/I and AMSR," Algorithm description of PIs for SSM/I and ADEOS-II/AMSR, 2nd AMSR Workshop, 61-1 - 61-9.
- Sato, Y., Y. Takeuchi and T. Tauchi, 2004: Use of TMI and SSM/I data in the JMA operational Meso Analysis., CAS/JSC WGNE Res. Act in Atmos. Ocea. Model.

¹ Japan Aerospace Exploration Agency

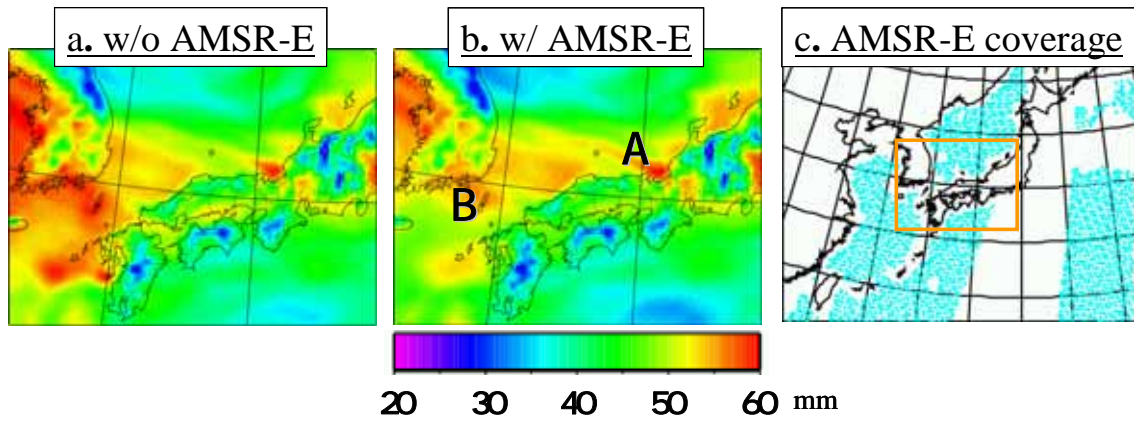


Fig. 1 (a) Analyzed TCPW field without the AMSR assimilation at 18UTC 17 July 2004. (b) Same as in (a) but with the AMSR-E assimilation. (c) The AMSR-E data coverage at the same time.

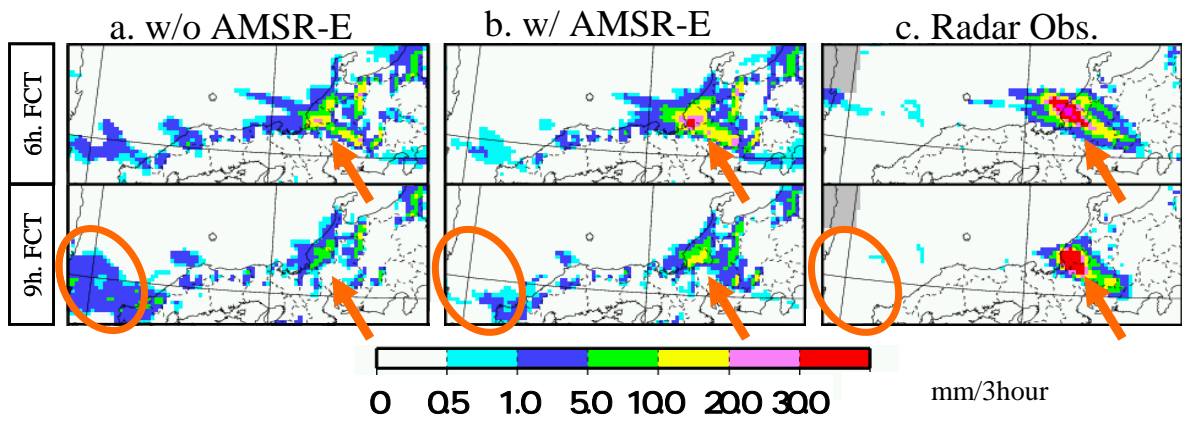


Fig. 2 (a) 3-hour rain forecasts after 6 hours (upper) and 9 hours (lower) from the initial condition of Fig.1 (a). (b) Same as in (a) but from the initial condition of Fig.1 (b). (c) 3-hour rain at 00UTC 18 July 2004 (upper) and 03UTC (lower) estimated by radar observation.

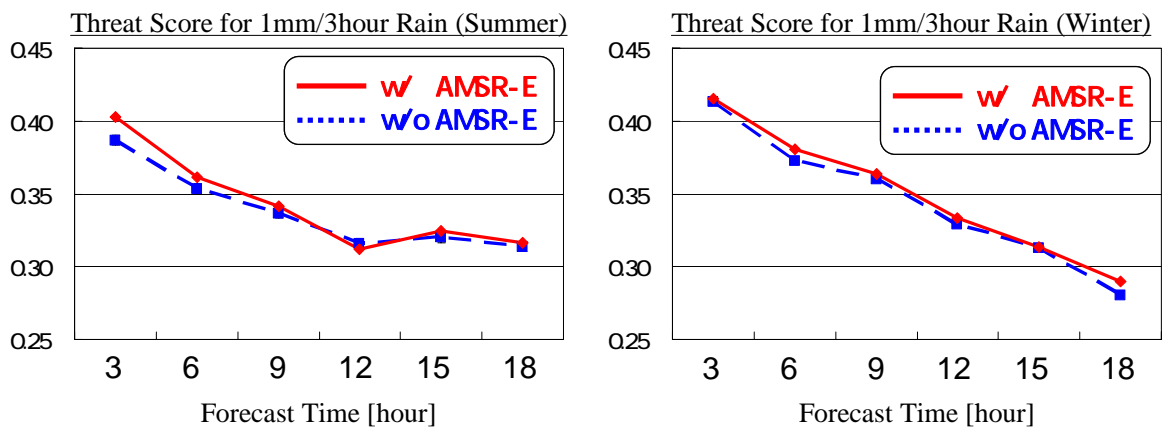


Fig. 3 (a) The threat scores for weak rainfall (1mm/3hour) forecasts in the case of summer 2004 (15 samples). (b) Same as (a) but in winter 2004 (15 samples).

Comparison of Two Tropical Cyclone Bogussing Schemes

DONGLIANG WANG*, XUDONG LIANG

Shanghai Typhoon Institute, China Meteorological Administration, Shanghai, China

*Email: wangdl@mail.typhoon.gov.cn

1. Introduction

Recently, the air force weather agency (AFWA) and NCAR (2001) proposed a scheme for bogussing TC into the initial condition of MM5 (Pennsylvania State University-National Center for Atmospheric Research non-hydrostatic Mesoscale Model version 5). And a litter earlier, Zou and Xiao (2000) developed a new bogussing approach by using a four dimensional variational data assimilation technique (4DVAR). Although these two schemes had improvements in different aspects of the bogussing technique, relatively few attempts have been made to systematically study their impact on numerical TC forecasts, particularly for those in the western North Pacific (WNP). The objective of this study is therefore to compare the impact of these two bogussing schemes.

2. Bogus data assimilation (BDA) and NCAR-AFWA (N-A) bogussing scheme

The BDA method includes: (1) prescribing an axisymmetric sea-level pressure (SLP) distribution from the Fujita formula; and (2) assuming temporal change of SLP is relatively small within 30 minutes so that the bogus SLP field is assimilated every two time steps.

The NCAR-AFWA bogussing scheme also includes two primary steps: (1) Once the first-guess vortex is located by searching the maximum vorticity, the vorticity, geostrophic vorticity and divergence are modified. Changes in the non-divergent stream function, geopotential and velocity potential are then computed, which are used to calculate a modified velocity field. (2) The bogus axisymmetric vortex with wind given by the Rankine vortex, nonlinear balanced mass and wind, and nearly saturated core is implanted into the background using a weight function.

3. Results and discussion

An example of the impact on the initial conditions is presented for the case of Rusa in its mature stage. The initial vortex becomes more intense and realistic, with the center of the maximum winds closer to the vortex center (Fig. 1a and 2a). A warm and wet core in the mid troposphere is adjusted by the N-A scheme (Fig. 2b and c). Meanwhile a more realistic vertical structure is obtained from BDA scheme, with a wet center near the low troposphere, and a warm core which becomes warmer and larger with increasing height until upper troposphere (Fig. 1b and c).

The results from the 41 cases occurring over the WNP in 2002 suggest that the adjustments in the initial structures cause improvements in TC track predictions (Fig. 3a). The mean 24-h position error for the BDA experiments is reduced from 175 to 121 km, and the 48-h error from 238 to 189 km, the reductions being 31% and 21%, respectively. The improvements for the N-A experiments occur however, only up to the 42-h prediction. The vortex in six cases has larger initial location and intensity errors after using N-A bogussing scheme, and with these six cases rejected, the mean track errors become smaller than

the CTRL experiments at all the forecast times. The improvements in the intensity forecasts are significant using BDA scheme, but it seems the N-A bogussing scheme has a negative impact on the intensity predictions.

The results show that the BDA scheme has better performance in both track and intensity forecasts, and although the initial wind fields in N-A scheme seem more reliable, they are unable to be maintained during integration.

References

Low-Nam, S., and C.Davis, 2001: Development of a tropical cyclone bogussing scheme for the MM5 system. *The Eleventh PSU/NCAR Mesoscale Model Users' Workshop, June 25-27, Boulder, Colorado*, 130-134

Zou X., and X. Qingnong, 2000: Studies on the initialization and simulation of a mature hurricane using a variational bogus data assimilation scheme. *J. Atmos. Sci.*, **57**:836-860

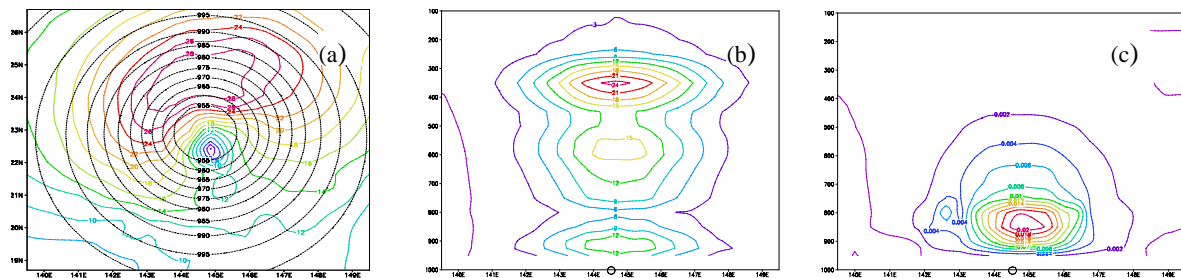


Fig. 1 (a) Distributions of SLP and wind speed fields at 850 hPa, and east-west cross section of (b) temperature and (c) specific humidity differences between CTRL and BDA

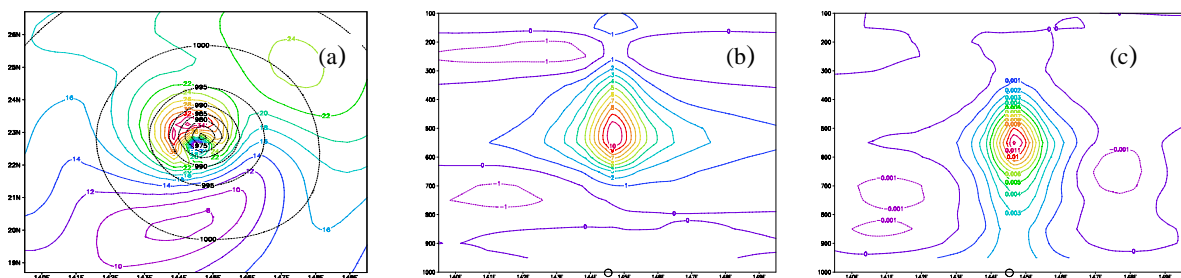


Fig. 2 Same as Fig. 1 but for N-A bogussing scheme

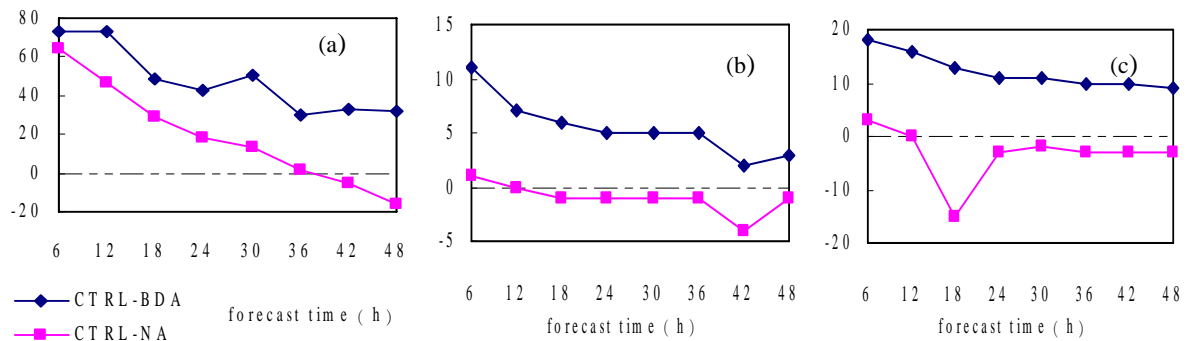


Fig. 3 Differences of forecast errors between CTRL and BDA or N-A scheme for (a) TC track (km), (b) maximum winds ($m s^{-1}$) and (c) MSLP (hPa)